

MAGNETIC FIELDS, PRESSURES, AND THERMALLY UNSTABLE GAS IN PROMINENT H I SHELLS

CARL HEILES

Astronomy Department, University of California, Berkeley

Received 1988 April 8; accepted 1988 June 28

ABSTRACT

We have measured B_{\parallel} using the Zeeman effect for the 21 cm line in emission for 73 positions located both in morphologically distinct H I shells and in a comparison region. The H I structures are filamentary instead of sheetlike. B_{\parallel} is typically $\sim 6.4 \mu\text{G}$ in morphologically prominent filaments and smaller elsewhere. In the filaments, magnetic pressure dominates thermal and turbulent gas pressures by factors of ~ 67 and ~ 10 , respectively, if our estimates of H I volume density are correct; line widths are typically ~ 1.8 times smaller than the Alfvén velocity. The magnetic pressure $B^2/8\pi \sim 4.7 \times 10^4 \text{ cm}^{-3} \text{ K}$. B_{\parallel} , as derived from the Zeeman effect, does not correlate with Faraday rotation.

In the process of deriving B_{\parallel} , we decomposed the H I spectrum for every position into Gaussian components. Most positions require a broad Gaussian, which presumably corresponds to the “warm neutral medium.” Full widths at half-maximum for many of these broad components imply temperatures less than a few thousand K, much smaller than the average FWHM for broad components. Gas at such temperatures is thermally unstable.

Subject headings: interstellar: magnetic fields — radio sources: 21 cm radiation — Zeeman effect

I. INTRODUCTION

For many years, we have been conducting observations of Zeeman splitting of the 21 cm line seen in emission with the 85 foot (26 m) paraboloid at Hat Creek Radio Observatory (HCRO). This paper reports on results for 73 positions, obtained with a total of 1327 hours of integration, during the period 1984 April 30 to 1988 April 18. We observed two types of region: H I shells and region A of Simard-Normandin and Kronberg (1980), which exhibits systematically large Faraday rotation measures (RMs) of extragalactic sources. In two H I shells, Troland and Heiles (1982*b*) found high field strengths, $> 6.7 \mu\text{G}$, and interpreted the results in terms of isothermal shock enhancement of the field strength and volume density; in the present paper, we extend these results to five well-defined shells. In region A of Simard-Normandin and Kronberg (1980), we find that Zeeman-derived magnetic fields do not correlate with RMs. Region A does not seem to be dominated by morphologically distinct H I shells and can be considered a crude “control region” to which H I shells can be compared.

We remind the reader that our observations are only sensitive to the line-of-sight component of the magnetic field, denoted herein by the symbol B_{\parallel} . The *a priori* probability that the total magnetic field strength B is larger than B_{\parallel} by a factor x is equal to $1/x$, and a randomly chosen group of positions has $B_{\parallel} = B/2$ (Heiles and Troland 1982). It is not generally possible to determine the field geometry, although in one case a correlation between B_{\parallel} and V_{LSR} was instructive (Heiles 1988).

II. TECHNICAL DETAILS

a) Observation Techniques

The observational techniques and difficulties have been described previously (Heiles 1988). Again, we have not performed the large computing job of calculating the contribution of the polarized sidelobes, which extend over very large solid angles in the sky. We have two reasons that justify this shortcoming. One, an empirical determination of the sidelobe con-

tribution (§ II*b*), shows that it is small. Two, the sidelobe contribution varies with season of the year. The observations reported herein extend over several years, and many positions have been observed at several different times of year. Each individual observation always agreed, within the noise, with other individual observations, and with the grand average of all observations.

On 1988 March 7 we discovered that the turnstile polarimeter was not perfectly adjusted. It had been in this state for an unknown period of time. This produced some sensitivity to linear polarization: the percentage polarization measured for a 100% linearly polarized signal would have been 7.8%. This introduced a small instrumental effect which may be important for the weaker signals at some of our positions. The telescope beam shape for a linearly polarized signal is elliptical, not circular, because the radiation pattern of the feed horn differs for directions parallel and perpendicular to the direction of polarization. Our V spectra are polarization-switched spectra; with the slightly elliptical beam (whose position angle differs by 90° for the two polarizations), the polarization-switched beam pattern contains four lobes, two positive lobes in the east-west direction and two negative lobes in the north-south direction, with lobe amplitudes of about 0.65% relative to the on-axis response of the telescope. This makes our V spectra contain a small residual of the second derivative of the 21 cm line brightness on the sky. This 0.65% amplitude can be compared to the peak-to-peak amplitude of the first derivative of the telescope beam (“beam squint”), which in our case was less than 0.2%. Second derivatives of the 21 cm line are considerably smaller than first derivatives, so that in the net this second-derivative effect is not usually larger than the beam squint effect.

Upon discovery of this maladjustment, the turnstile was properly adjusted and repeat measurements taken of a number of positions. The results agreed perfectly with the previous measurements. We have not carried out the extensive work necessary required to check all of our results on an individual basis. However, we can estimate the order of magnitude of this

instrumental contribution from knowledge of the second derivative of the 21 cm line brightness. The effect should be negligible for all except the weakest signals at most positions.

For nearly all positions, the total bandwidth was 625 kHz, covered by two independent autocorrelators each with 512 channels, providing a total velocity coverage of 132 km s^{-1} and an interchannel separation of 0.26 km s^{-1} ; for a few positions, including G64.2 – 10.6 (Fig. 1c), the total bandwidth was twice as large, 1.25 MHz.

All of our data are presented as Stokes parameter I or Stokes parameter V spectra. I is the total intensity, and V is the difference between the two circular polarizations, equal to left-hand circular *minus* right-hand circular (LCP – RCP, in the IEEE definition, in which RCP is defined as clockwise rotation of the electric vector as seen from the transmitter of the radiation; Kraus 1966). This convention has also been used in several of our previous publications (Troland and Heiles 1982b; Heiles and Troland 1982; Heiles 1988).

b) Empirical Estimate of Contribution of Polarized Sidelobes

Polarized sidelobes tend to vary rapidly with azimuthal angle measured relative to the telescope beam center. Thus, an estimate of the contribution of polarized sidelobes can be obtained by measuring V spectra with different azimuthal

orientations of the sidelobes relative to the sky. This is easily done with altitude-azimuth mounted telescopes. However, the HCRO telescope is equatorially mounted, so this can be done only at one position on the sky: the north celestial pole (G123.0+27.2). We took such measurements by pointing the telescope at the pole at zero hour angle and continually recording the spectra averaged over 2 hr, obtaining measurements centered at 12 right ascensions with average integration times at each right ascension of 9.0 hr. A complete analysis of these data, to be performed in the future, will enable us to check the accuracy of our calculations of the contributions of polarized sidelobes. However, such an analysis is unnecessary for the present paper, because the sidelobe contribution is small.

For the $V_{\text{LSR}} = -4.9 \text{ km s}^{-1}$ component reported in Table 1, the average B_{\parallel} was $+10.6 \mu\text{G}$, and the 1σ fluctuation among the 12 right ascensions was $1.7 \mu\text{G}$. This is an overestimate of the true fluctuation because of the limited integration time at each right ascension. We Fourier-decomposed the measured values according to right ascension: the amplitude of the first and second Fourier components (24 and 12 hr periods) were 0.9 and $1.1 \mu\text{G}$, respectively, with a phase difference of 72° ; the four higher order components were apparently noise with average amplitudes of $0.42 \mu\text{G}$.

Without performing calculations of the contribution of po-

TABLE 1
GAUSSIAN COMPONENTS FOR THE NCP SHELL

(l, b)	B	dB	T_a	V_{LSR}	FWHM	RM	t	Comments
(123.0, 27.2).....	10.6	0.7	11.6	-4.9	4.4	+2	107.6	-, 2
	5.2	0.9	11.6	-2.5	7.8	+2	107.6	-, 2
	-2.7	2.3	6.1	-16.2	13.0	+2	107.6	1, 2
	16.9	15.3	0.9	-31.4	14.4	+2	107.6	1, 2
(125.2, 31.8).....	11.6	0.8	35.6	0.6	5.6	+8	2.1	-
	-14.3	19.3	3.5	-6.7	28.3	+8	2.1	1
(125.5, 37.2).....	7.6	0.4	25.4	6.8	5.3	+1	51.8	-
	28.4	7.8	3.2	1.0	23.2	+1	51.8	1
(131.3, 42.6).....	6.4	1.1	8.6	6.2	5.5	+1	19.3	-
	25.7	5.4	3.6	5.0	22.1	+1	19.3	1
(135.3, 40.8).....	4.9	1.2	22.4	3.2	4.3	+3	2.1	-
	20.1	4.0	10.0	4.3	9.4	+3	2.1	1
(141.1, 42.0).....	-0.5	0.9	14.5	3.6	5.6	-3	11.0	-
	-9.7	10.1	2.3	2.9	16.6	-3	11.0	1
(142.6, 38.4).....	9.2	0.8	14.8	2.7	4.0	-6	16.8	-
	17.2	1.3	13.9	4.2	9.5	-6	16.8	1
(146.6, 42.6).....	0.3	0.9	16.9	3.7	4.5	-7	14.5	-
	19.8	2.0	11.2	2.7	10.5	-7	14.5	1
(151.2, 33.6).....	2.5	1.2	10.9	0.3	5.2	+3	12.7	-
	11.8	7.5	3.0	0.7	16.3	+3	12.7	1
(153.8, 36.0).....	5.2	0.9	12.2	0.1	7.0	+19	23.6	-
	12.0	4.5	3.9	-1.2	19.6	+19	23.6	1
(154.3, 36.6).....	1.1	0.4	15.2	0.2	4.6	+19	45.8	-
	-0.6	2.8	4.5	-0.9	16.8	+19	45.8	1
(157.4, 36.0).....	6.7	1.1	10.2	0.2	5.3	+12	15.6	-
	-11.9	4.5	4.3	-0.7	15.4	+12	15.6	1
(159.5, 36.0).....	1.8	0.9	20.1	1.3	3.5	+12	4.0	-
	10.2	4.2	7.9	0.1	12.2	+12	4.0	1

NOTE.—In the column headings, l is Galactic longitude, b Galactic latitude (both in degrees); B and dB are the line-of-sight magnetic field and its 1σ error, in microgauss; T_a is the antenna temperature of the peak of the Gaussian in kelvins; V_{LSR} is the LSR velocity of the Gaussian and FWHM the width of the Gaussian (both in km s^{-1}); RM is the rotation measure from Spoelstra 1972; and t is the integration time in hours. Entries in the "Comments" column denote the following: -, considered reliable; 1, considered unreliable because Gaussian is too weak and/or broad; not shown on figures; 2, North Celestial Pole.

larized sidelobes, we cannot tell whether this sidelobe contribution is representative of the other positions discussed here. We suspect that the contribution is abnormally large at the north celestial pole, because the V_{LSR} of the -4.9 km s^{-1} Gaussian component changes rapidly with position. If it is representative, then the errors in our derived values of B_{\parallel} are dominated by the sidelobe contribution, because the $1.7 \mu\text{G}$ 1σ sidelobe contribution is larger than the typical 1σ error reported in our tables. Nevertheless, for many table entries, the derived B_{\parallel} is comfortably larger than $1.7 \mu\text{G}$.

c) *Sample Profiles, Least-Squares Fits, and Multicomponent Profiles*

All values of B_{\parallel} are derived using a least-squares fitting procedure. This procedure provides a formal 1σ error in the derived B_{\parallel} . Troland and Heiles (1982a) found that an individual result could usually be trusted if the derived B_{\parallel} was at least 3 times the 1σ error (as is usual for statistically derived quantities). Nevertheless, the 1σ error is a more useful quantity when comparing aggregates of measurement. In this paper, we quote 1σ errors, but do not regard individual measurements as being statistically significant unless B_{\parallel} exceeds the 1σ error by a factor of at least 3.

B_{\parallel} for a simple, single-peaked profile can be fitted using the usual procedure, which fits the V profile to the S-shaped frequency derivative of the I profile. However, many of the positions observed do not have simple, single-peaked I profiles. The multiple peaks are, at least in some cases, produced by unrelated structures that happen to lie along the same line of sight. There is no reason why these structures should have the same B_{\parallel} . For example, in the classical case of the Perseus arm absorption feature of Cas A, the discovery case for interstellar Zeeman splitting, the feature has two components whose values of B_{\parallel} differ by a factor of nearly 2 (Verschuur 1969). It is necessary to derive B_{\parallel} values for multiple peaks independently. To do this, we decompose the I profiles into multiple Gaussian components and simultaneously fit the V spectrum to frequency derivatives of the Gaussian components, allowing a different B_{\parallel} for each component.

Poor signal-to-noise is a characteristic of most of our V spectra because of limited integration time. Furthermore, instrumental effects are present at some level in every V spectrum. In two situations we do not consider our technique, which involves Gaussian decomposition, reliable. These are cases in which the decomposition of the I spectrum is uncertain because the components are blended, and cases involving broad, weak components.

This latter situation is especially common. Almost no single-peaked I profile can be well fitted by a single Gaussian, because the profiles have broad wings. Two Gaussians, one wide and one narrow, having nearly the same central velocity, usually reproduce the I spectrum very well. These presumably correspond to the "cold neutral medium" and "warm neutral medium," which are distinguishable in H I absorption studies not only by their line widths but by their gas temperatures (Kulkarni and Heiles 1987, 1988, hereafter KH). The B_{\parallel} derived for the wide component is, in our opinion, unreliable. Its value is often large, and often the formal error is not large, so that, from a purely statistical standpoint, the fit is acceptable.

We illustrate the uncertainty of B_{\parallel} derived from a fit to a broad, weak Gaussian component in Figure 1a (also see Table

2). Owing to accidental overscheduling in various observing periods, G270.8+40.5 received 58.9 hr of integration time between 1989 October 18 and 1986 May 9. This position has a single-peaked I profile, and the V profile exhibits a well-defined, very sharp "S"; for the narrow Gaussian component, $B_{\parallel} = -5.3 \pm 0.3 \mu\text{G}$. The V spectrum also exhibits broad structure at the 0.005 K level, negative on one side and positive on the other. This is exactly the result expected for real Zeeman splitting of the broad, weak Gaussian component; for this component, the formal fit provides $B_{\parallel} = -14.3 \pm 3.5 \mu\text{G}$. However, the V spectrum clearly contains other systematic, instrumental effects. First, there is a broad baseline wiggle at the 0.005 K level; this is probably electronic in origin. Second, there must be a contribution from distant circularly polarized sidelobes at some level; we have not estimated this contribution, but it is apparently very small for this position. Finally, there is weak interference at the extreme right-hand edge of the profile, generated on the HCRO site at a local frequency of 1420.000 MHz; this should not produce any effect whatsoever on the remainder of the spectrum. (This interference does not appear in all of our data. To expunge it from this spectrum would have significantly reduced the available integration time.)

Multiple components produce additional uncertainty. G96.8-19.6 (Fig. 1b; Table 4) required four Gaussian components for a satisfactory fit. The V spectrum, with 43.2 hr of integration, reveals an "S" with about 0.09 K peak-to-peak amplitude for the 1.1 km s^{-1} component ($B_{\parallel} = +8.4 \pm 0.5 \mu\text{G}$) and a barely detectable "S", with about 0.01 K amplitude, for the -22.3 km s^{-1} component ($B_{\parallel} = +4.1 \pm 1.5 \mu\text{G}$; this result is not statistically significant). Both components are well defined and isolated from other components. However, the 3.5 km s^{-1} component ($B_{\parallel} = +18.3 \pm 1.0 \mu\text{G}$) is both broad and not well isolated. Even though the formal statistical significance of the derived field is high, and even though the broad, negative-going tail on the positive-velocity end of the V spectrum is definitely detected, we do not regard the derived B_{\parallel} for the 3.5 km s^{-1} component as reliable, because of blending.

Nearly all V spectra, even those with multiple components, were well fitted by our technique of Gaussian fitting. Five were not; these are denoted in the tables as possibly containing structure in the V spectrum. An example is G64.2-10.6 (Fig. 1c; Table 4). The I spectrum is well fitted by three Gaussian components. The V spectrum exhibits a clearly detectable signal with a -, +, - pattern. However, the pattern cannot be matched to Zeeman splitting of the Gaussian components: only the leftmost peak in the I spectrum is well fitted, with $B_{\parallel} = +9.9 \pm 1.9 \mu\text{G}$. This may indicate that the rightmost peak in the I spectrum is really composed of two narrower Gaussians, only one of which has a detectable B_{\parallel} . The Gaussian components of both peaks in the I spectrum are blended; we have an uneasy feeling about this particular fit, but nevertheless adopt the derived B_{\parallel} for the leftmost peak reliable.

In this paper we list in tabular form the parameters for all Gaussian components at each position, because this is a relatively compact form in which to present the data. However, the derived B_{\parallel} values for many of the components are unreliable for the reasons discussed above, even though formally speaking they are statistically significant. The offending values of B_{\parallel} are noted in each table. Faraday rotation measures are also listed in the tables if they are available from the literature.

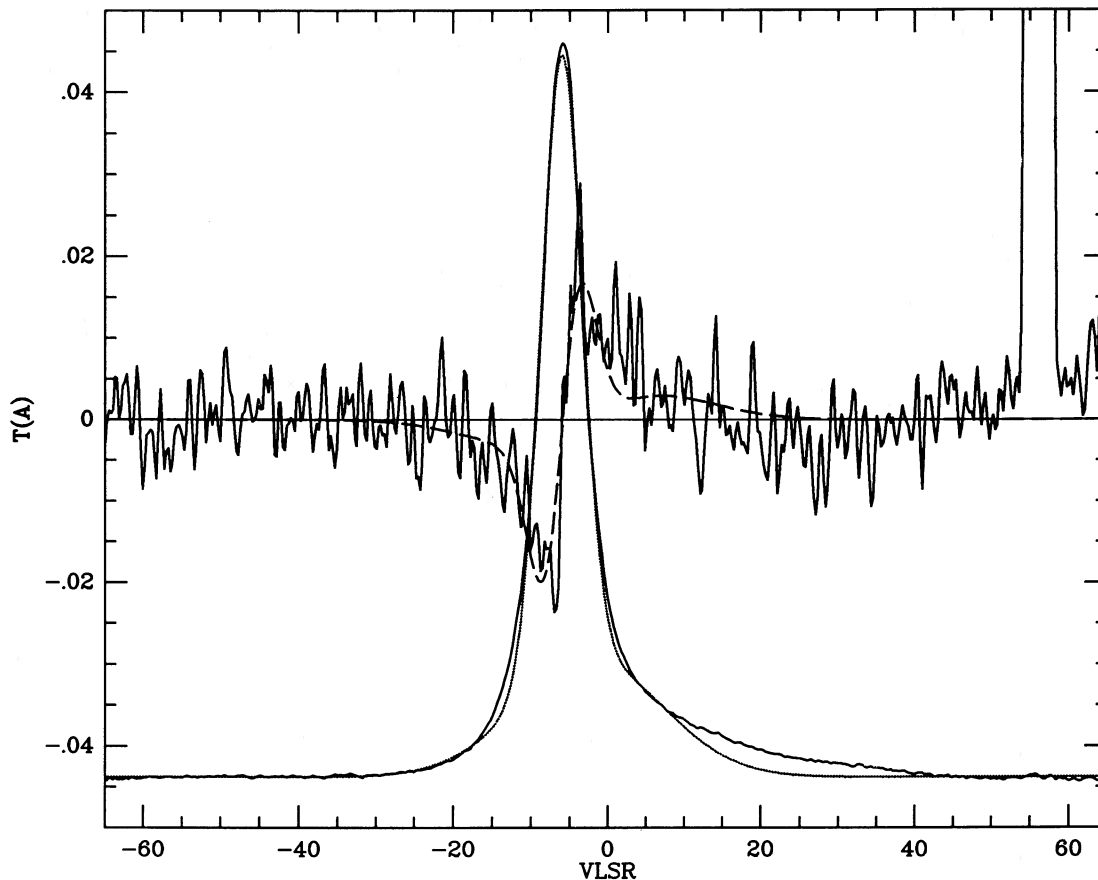


FIG. 1a

FIG. 1.—(a) Spectra for G270.8 + 40.5, illustrating the unreliability of fits to broad, weak components resulting from instrumental effects. The smooth solid line is the frequency-switched (Stokes parameter I) spectrum; the dotted line adjacent to it is the least-squares fit to two Gaussian components. The noisy solid line is the polarization-switched (Stokes parameter V) profile, and the dashed line following it is the least-squares fit to the frequency derivative of the Gaussian components that fit the I profile. The off-scale signal at the right-hand edge of the V profile is interference (see text). Gaussian components and derived B_{\parallel} 's are given in Table 3. (b) Spectra for G96.8 - 19.6, illustrating the difficulties of fitting blended multiple components. The smooth solid line is the frequency-switched (Stokes parameter I) spectrum; the dotted line adjacent to it is the least-squares fit of four Gaussian components. The noisy solid line is the polarization-switched (Stokes parameter V) profile, and the dashed line following it is the least-squares fit to the frequency derivative of the Gaussian components that fit the I profile. Gaussian components and derived B_{\parallel} 's are given in Table 4. (c) Spectra for G64.2 - 10.6, illustrating a typical case of blended components for which multiple Gaussians do not accurately reproduce the V profile. The smooth solid line is the frequency-switched (Stokes parameter I) spectrum; the dotted line adjacent to it is the least-squares fit of three Gaussian components. The noisy solid line is the polarization-switched (Stokes parameter V) profile, and the dashed line following it is the least-squares fit to the frequency derivative of the Gaussian components that fit the I profile. Gaussian components and derived B_{\parallel} 's are given in Table 3.

III. THE NORTH CELESTIAL POLE LOOP (GS 135 + 38 + 5)¹

This is a relatively small elliptical loop, about $21^{\circ} \times 12^{\circ}$ ($l \times b$), which runs through the north celestial pole (NCP). In the Colomb, Pöppel, and Heiles (1980) maps, it is visible at velocities between 0 and 13 km s^{-1} , with no discernible change of size with velocity. The inside of the loop is devoid of H I, because $N_{\text{H I}}$ inside the loop is about the same as that above the loop (Heiles 1975). This strongly suggests that this structure is not a shell but a filament. The filament is about 2.5 in width. In addition, this region is permeated by "intermediate-velocity" H I at $\sim -50 \text{ km s}^{-1}$. In no case did we measure a significant magnetic field for this gas, nor were any properties of this gas correlated with those of the low-velocity gas. Thus the intermediate-velocity gas is irrelevant for the purposes of the present paper, and we disregard it henceforth.

¹ The three numbers in the GS notation are longitude, latitude, and V_{LSR} , respectively (Heiles 1979).

We have measured the field strength at 12 positions in and near this filament. Some of these positions, the ones having $l \gtrsim 150^{\circ}$, may lie outside the filament in more smoothly distributed gas. Figure 2 (Plate 25) shows the H I column density integrated between -35 and $+35 \text{ km s}^{-1}$ in a gray-scale format, together with B_{\parallel} for the narrow component. The H I data are from Heiles and Habing (1974); the white rectangle is the north celestial pole, where data of this survey do not exist. The field strength is proportional to the size of the plus sign on Figure 2, while the 1σ error in the derived field is proportional to the size of the circle. One or two of the symbols are difficult to see because of low contrast with the gray-scale representation. Table 1 presents the positions and column densities numerically.

Most of the I profiles were reasonably well represented by one Gaussian component. However, all I profiles have long tails, relative to a single Gaussian component. A two-component fit reproduced these tails fairly well. One component was narrow, with (average FWHM, standard

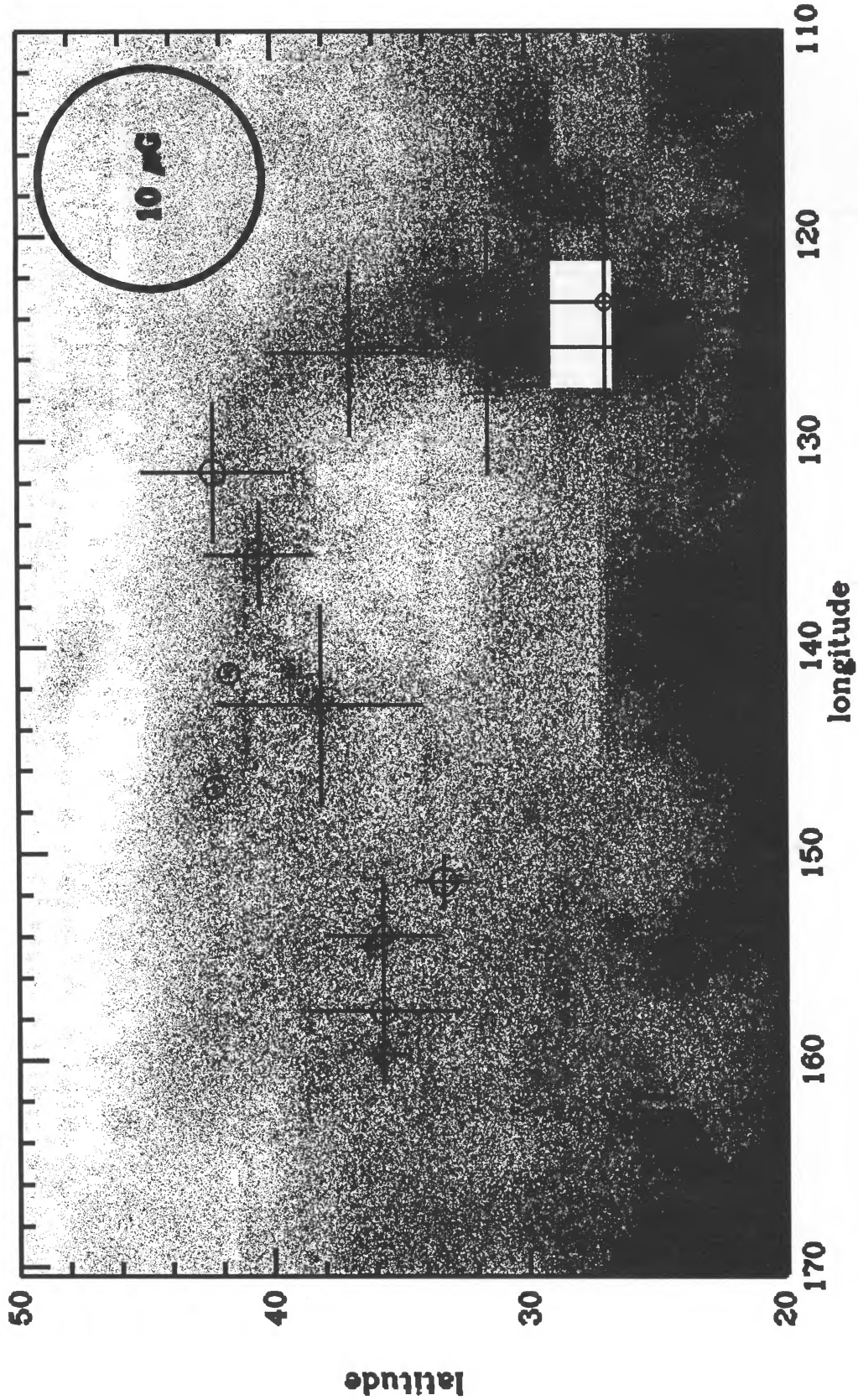


FIG. 2.—Map of the NCP H I shell, showing $N_{\text{H I}}$ between -35 and $+35 \text{ km s}^{-1}$ and derived B_l 's from Table 1. Plus signs indicate positive B_l 's, cross indicates negative B_l , with size proportional to the value; circles indicate the 1σ error. The white rectangle is centered on the north celestial pole, where the Heiles and Habing (1974) survey provides no data. Higher quality H I maps can be found in Colomb, Pöppel, and Heiles (1980) and Heiles (1984a).

HEILES (see 336, 811)

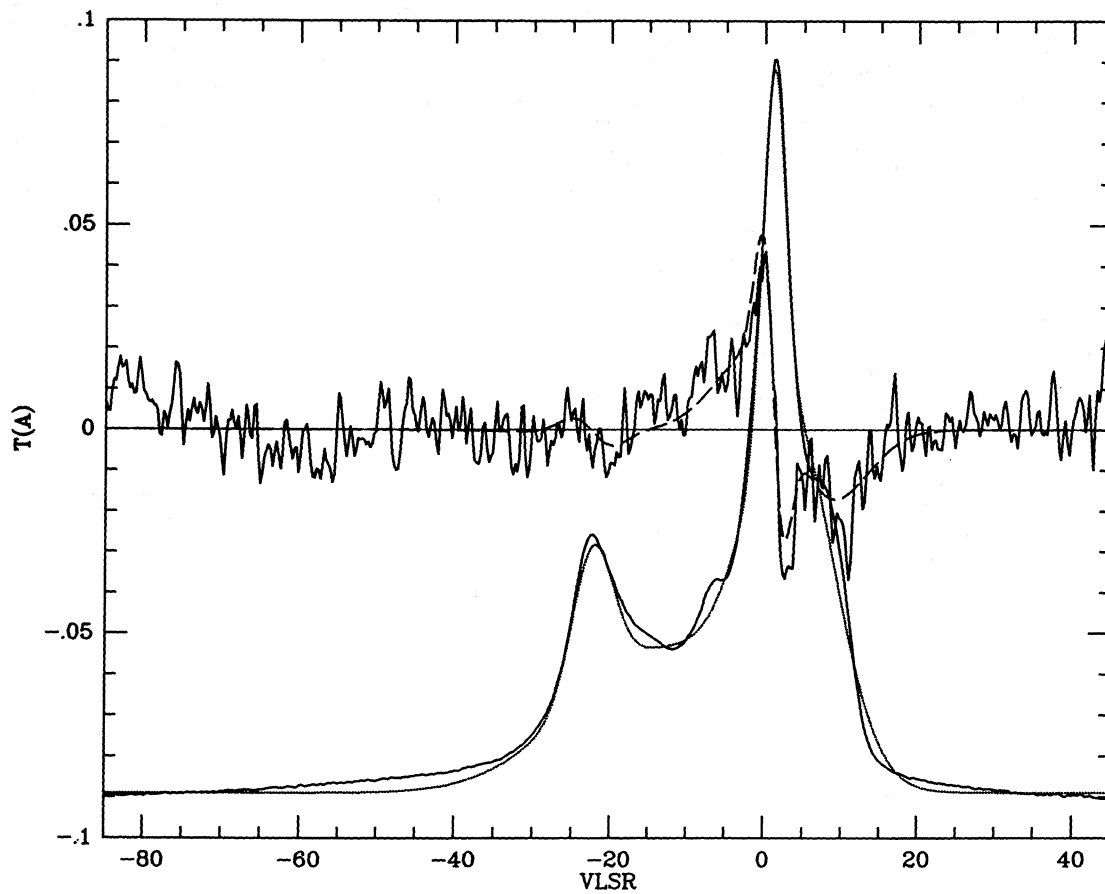


FIG. 1b

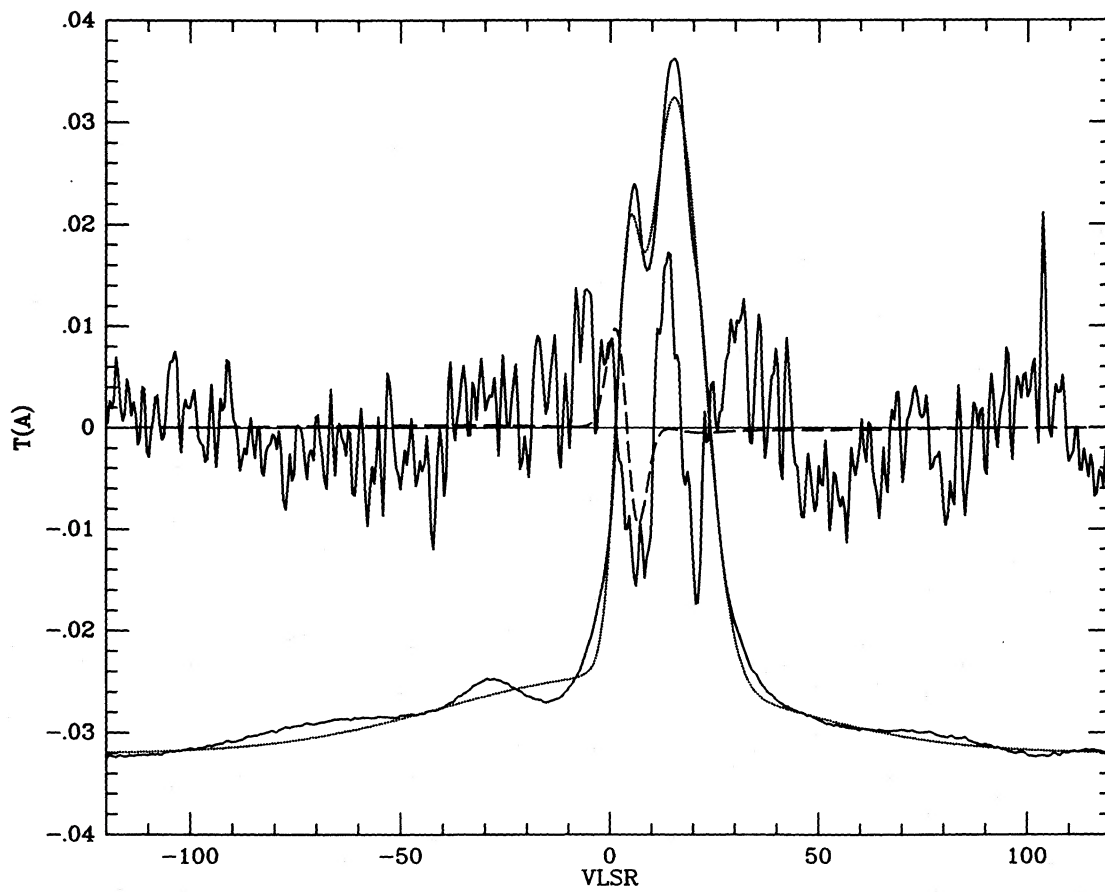


FIG. 1c

deviation) of (5.0, 0.9) km s^{-1} ; the other was wide, with (16.7, 5.9) km s^{-1} . The (average central V_{LSR} , standard deviation) were (2.4, 2.4) and (0.9, 3.2) km s^{-1} , respectively, for the two components. An easily detectable B_{\parallel} was found for seven of the narrow components and five of the wide components. All statistically significant fields were positive. The average field strengths were 7.2 and 21.3 μG for the narrow and broad components, respectively.

The large B_{\parallel} for the wide components is unreliable (§ IIc). Nevertheless, the fact that the derived field strengths for the broad components show consistency for several adjacent positions suggests that the results may, in fact, be real. If they are real, then B_{\parallel} is typically higher in the broad component. This would be surprising, because the broad component is presumably warmer than and less dense than the narrow component. To determine definitively the reality of the results for the broad component requires a significantly larger observational effort than is contained in the present paper. Such an effort is in progress and will follow the procedure outlined in § IIb.

For the narrow components there is no statistically significant correlation of field strength with H I column density. However, the four positions having $B_{\parallel} < 3 \mu\text{G}$ have relatively low column densities. Figure 2 shows that one, G141.1+42.0, is near the outer edge of the filament. The others are located fairly far outside the inner edge of the loop in a region where the filament is not morphologically well defined; most of the H I at these positions may lie altogether outside the filament.

The consistent positive values of field in this region, together with the relatively large values of field strength, show that the field cannot lie closely orthogonal to the line of sight. This suggests that we might see the field in Faraday rotation data. Unfortunately, this is not the case. The map of extragalactic RMs by Simard-Normandin and Kronberg (1980) shows only three sources in the area. Two have negative and one positive RM, so any correspondence is indeterminate. Spolestra's (1972) map of RMs determined from diffuse Galactic synchrotron radiation shows RMs varying from -6 to $+6 \text{ rad m}^{-2}$ along the filament in which we measure consistently positive values of B_{\parallel} ; values are given in Table 1. There is no correlation of B_{\parallel} and RM. With our observed B_{\parallel} values of order $10 \mu\text{G}$, an RM of 6 rad m^{-2} is produced by an electron column density of only $0.8 \text{ cm}^{-3} \text{ pc}$. This is much smaller than the total electron column densities observed for high-latitude pulsars, and is easily produced in a few-pc diameter cloud having the electron density of $\sim 0.4 \text{ cm}^{-3}$ that resides at high $|z|$'s (KH).

H I column densities for positions centered on the filament average about $4 \times 10^{20} \text{ cm}^{-2}$. If the length of the filament along the line of sight is the same as that across the line of sight, and if its distance is 200 pc, then $n_{\text{H I}} \approx 15 \text{ cm}^{-3}$.

IV. THE NORTH POLAR SPUR LOOP (GS 314+17+5)

The North Polar Spur (NPS) forms part of a 116° diameter small circle on the sky called Loop I by radio astronomers (see Berkhuijsen, Haslam, and Salter 1971). It is centered at $(l, b) \approx (329^\circ, 17^\circ 5')$. The radius of this shell is 115 pc, and its central distance is 130 pc (Berkhuijsen 1973). Heiles *et al.* (1980) compare the structure of the region in diffuse soft X-ray emission, radio continuum, and H I.

The H I maps of Colomb, Pöppel, and Heiles (1980) show that part of the region has the observational signature of an expanding H I shell, with a "polar cap" at the most extreme

negative velocity and progressively larger rings of H I at less extreme negative velocities. The "polar cap" is visible near $V_{\text{LSR}} = -30 \text{ km s}^{-1}$ and is centered near $(l, b) \approx (300^\circ, -10^\circ)$, about 40° distant from the center of the NPS. It gradually increases in diameter for more positive velocities, although its structure is very patchy. Near $V_{\text{LSR}} = 0 \text{ km s}^{-1}$, the H I is centered $\sim 15^\circ$ lower in l than the NPS but at roughly the same b . At positive V_{LSR} 's, only fragments of the H I can be seen.

We have observed 28 positions in this region. These positions tend to be near the edge of the shell, because most of the central portions lie at low declinations and are either inconvenient or impossible to observe from HCRO. Because of the location near the edge, the measured V_{LSR} 's tend to be close to zero. Nevertheless, most of the gas should lie within the expanding H I shell.

Figures 3a and 3b (Plates 26–27) show the H I column density integrated between -35 and $+35 \text{ km s}^{-1}$, together with the derived magnetic field strengths and limits for the strong narrow components near $V_{\text{LSR}} = 0 \text{ km s}^{-1}$. We present two figures to cover the whole region with adequate scale. Most of the l profiles are well represented by two Gaussians, a narrow and a broad component centered near $V_{\text{LSR}} = 0 \text{ km s}^{-1}$. At 10 positions other components are seen, all with $V_{\text{LSR}} > 10 \text{ km s}^{-1}$; at one of these 10 positions, a -16.8 km s^{-1} component is also seen. These nonzero-velocity components are always weak, with peak antenna temperatures never larger than 5.8 K, and relatively broad; this makes any derived B_{\parallel} 's suspect, for the reasons outlined in § IIc. In no case was a statistically significant value for B_{\parallel} derived. Numerical results for all components are given in Table 2. Within the errors, our results agree with those of Troland and Heiles (1982a) at four of their positions that lie near three of ours; they used the same telescope but different electronics. This is the only portion of the region that does not exhibit detectable B_{\parallel} 's; Troland and Heiles (1982a) were unlucky in their choice of position, which was unfortunate because the work was a portion of Troland's Ph.D. thesis.

Figure 3a, which covers the longitude range from 240° to 340° , shows predominantly negative fields. In contrast, Figure 3b shows positive fields from $l \sim 335^\circ$ to $l = 20^\circ$, and both positive and negative fields near $l = 35^\circ$. Twenty-seven additional positions located near $(l, b) = (7^\circ, 20^\circ)$ all have positive values of field, with B_{\parallel} averaging $\sim 4 \mu\text{G}$ (Heiles 1988).

The H I-derived B_{\parallel} 's have no correspondence in Faraday rotation data. Between $l \approx 270^\circ$ and $l = 15^\circ$, the extragalactic source RMs of Simard-Normandin and Kronberg (1980) are predominantly negative at the values of b of interest here, corresponding to positive fields; our derived B_{\parallel} 's are primarily positive at the smaller longitudes and negative at the larger ones. For $l \gtrsim 15^\circ$, most of the RMs are positive both as derived from extragalactic sources and as derived from the diffuse Galactic synchrotron radiation (Spolestra 1971). Spolestra's RMs, given in Table 2 for all available positions, mostly imply B_{\parallel} values that are opposite in direction to our Zeeman-derived values.

The longitude dependence of the signs of our B_{\parallel} 's does correspond, roughly, to the dependence of the signs of RMs at negative Galactic latitudes, from which the overall Galactic field is determined (see Heiles 1987). The change in overall field direction from negative to positive near $l \approx 335^\circ$ corresponds reasonably well to the expected change in sign for the local Galactic field, which points roughly toward $l = 90^\circ$ with an uncertainty of some 15° . This situation is consistent with the

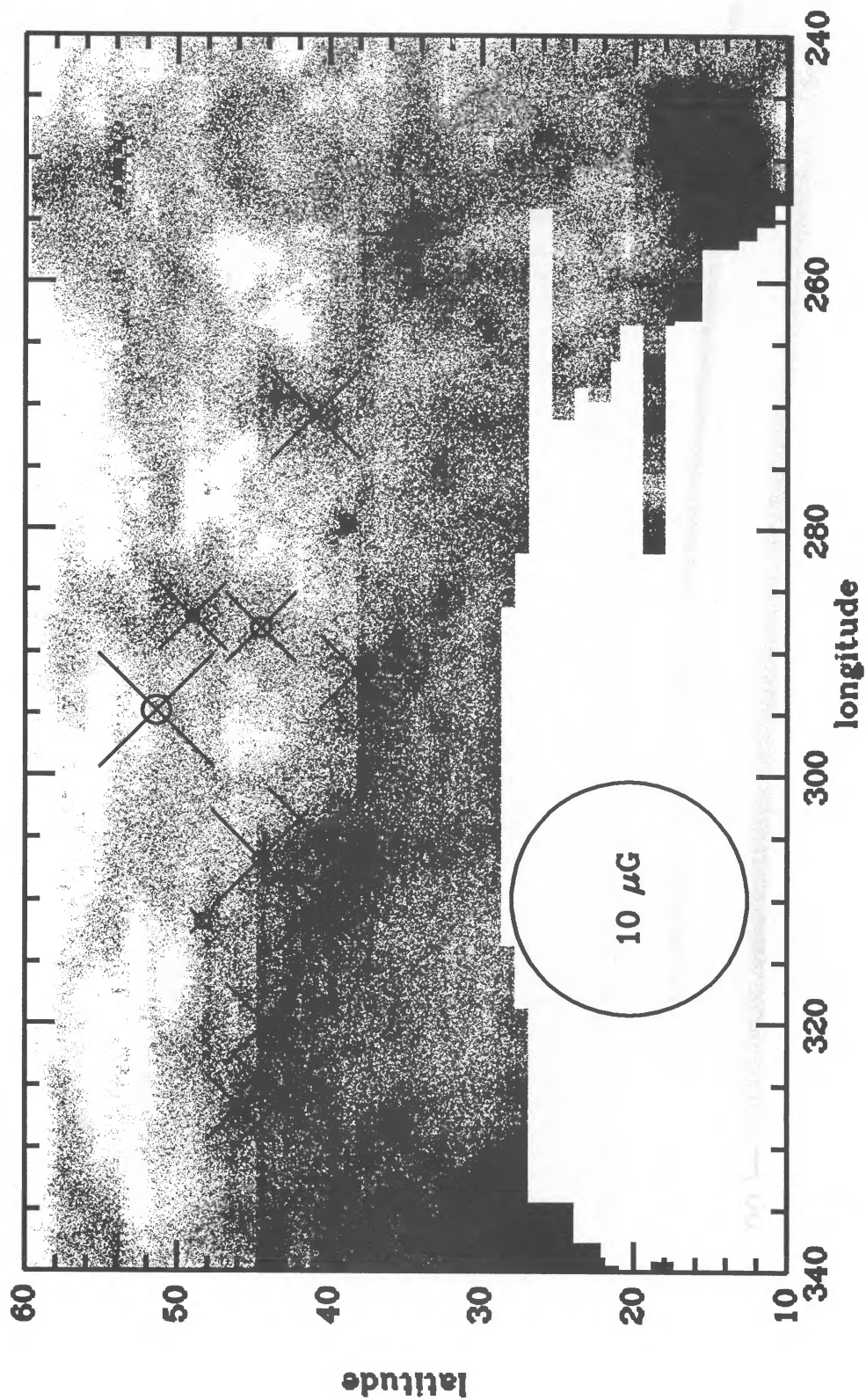


FIG. 3a

FIG. 3.—(a, b) Map of the NPS H I shell, showing N_{HI} between -35 and $+35 \text{ km s}^{-1}$ and derived B_{\parallel} ; crosses indicate negative B_{\parallel} , with size proportional to the value; circles indicate the 1σ error. The whole area is split into two figures for clarity. The large white area near the bottom of the figures has declination $\lesssim -30^\circ$, where the Heiles and Habing (1974) survey provides no data. Higher quality H I maps can be found in Colomb, Pöppel, and Heiles (1980) and Heiles (1984a).

HEILES (see 336, 813)

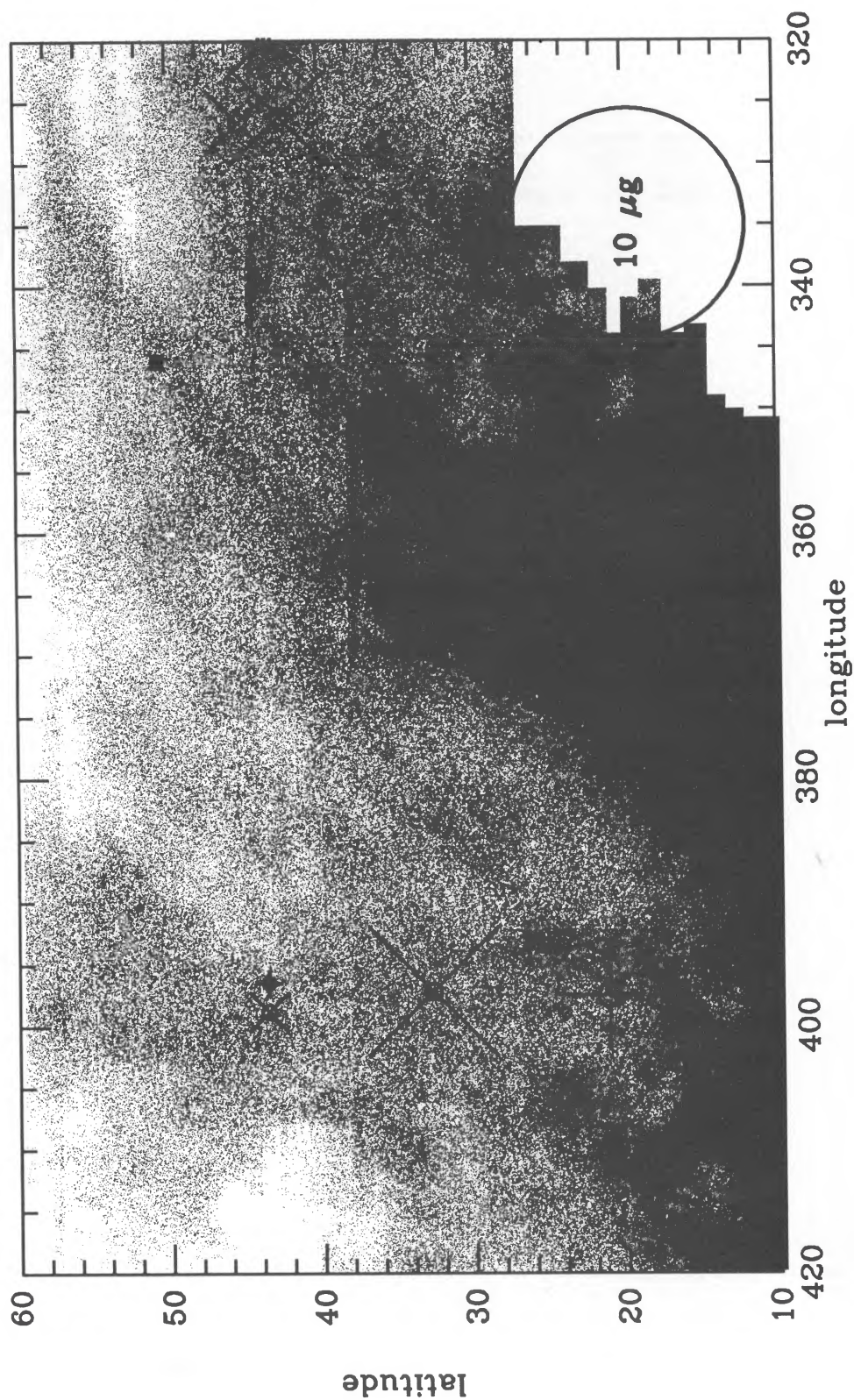


FIG. 3b

HEILES (see 336, 813)

TABLE 2
GAUSSIAN COMPONENTS FOR THE NPS SHELL

(l, b)	B	dB	T_g	V_{LSR}	FWHM	RM	t	Comments
(256.2, 34.2).....	4.2	0.4	24.1	-5.1	4.9	...	22.5	-
	-7.3	2.3	7.3	-3.0	15.9	...	22.5	1
	10.3	3.8	4.8	32.2	11.1	...	22.5	-
(269.4, 43.2).....	1.5	0.5	21.3	-6.9	4.7	...	21.7	-
	-14.6	2.1	8.1	-6.5	14.5	...	21.7	1
(270.8, 40.5).....	-5.3	0.3	24.0	-6.0	6.3	...	58.9	-
	-14.3	3.5	4.5	-2.0	24.3	...	58.9	1
(279.6, 38.4).....	-1.0	0.6	16.0	-5.5	4.9	...	19.9	-
	-0.4	3.0	5.8	-5.2	16.2	...	19.9	1
(287.2, 48.6).....	-4.0	0.5	26.7	-3.8	5.7	...	5.8	-
	-5.7	8.3	3.4	-4.4	21.5	...	5.8	1
(288.1, 44.1).....	-4.2	-0.8	23.3	-3.6	5.5	...	4.6	-
	22.3	11.6	3.2	-4.4	20.0	...	4.6	1
(291.7, 37.8).....	-4.3	0.4	16.9	-2.0	3.6	...	15.7	-
	-8.6	3.5	4.5	-1.7	15.4	...	15.7	1
	-6.6	3.2	2.3	-16.8	3.7	...	15.7	-
	0.9	2.5	3.9	16.3	6.6	...	15.7	-
(294.8, 51.0).....	-6.9	1.2	11.9	-4.5	4.4	...	7.8	-
	5.8	3.8	6.3	-3.5	12.5	...	7.8	1
(305.0, 40.5).....	-5.7	0.7	24.4	-3.8	4.5	...	17.1	-
	-4.9	2.7	10.6	-3.5	14.2	...	17.1	1
(306.8, 44.2).....	-5.8	0.6	24.8	-4.3	4.4	...	11.6	-
	-4.2	2.7	9.0	-4.1	13.3	...	11.6	1
	-1.3	3.9	3.7	29.3	5.4	...	11.6	-
(310.4, 40.2).....	-5.7	0.8	22.2	-5.1	5.2	...	5.3	-
	6.4	6.0	6.5	-4.5	23.7	...	5.3	1
	-7.5	2.3	5.8	0.4	2.7	...	5.3	2
(311.8, 48.0).....	-1.4	0.6	17.3	-5.5	3.7	...	9.6	-
	1.3	2.1	9.5	-3.5	12.4	...	9.6	1
(320.1, 43.8).....	-4.8	0.5	19.5	-5.5	3.9	...	15.1	-
	-2.7	1.3	13.4	-3.6	13.8	...	15.1	1
	5.4	3.8	5.2	23.0	16.4	...	15.1	-
(326.3, 42.9).....	-5.8	0.7	17.1	-4.7	4.8	...	18.4	-
	-5.6	1.5	13.6	-3.5	14.8	...	18.4	1
	6.6	5.8	2.9	17.0	12.3	...	18.4	1
(326.8, 45.6).....	-3.9	0.7	19.0	-4.8	4.7	...	11.6	-
	2.3	2.3	10.0	-3.5	16.7	...	11.6	1
	0.4	3.6	4.7	20.6	10.2	...	11.6	-
(339.5, 44.1).....	2.2	0.6	31.6	-2.9	7.8	...	10.7	3
	-7.9	4.3	3.3	18.5	6.2	...	10.7	1
	-10.2	4.1	7.4	-0.5	21.6	...	10.7	1
(346.2, 51.0).....	-0.9	0.5	23.0	-1.6	5.8	...	16.9	-
	11.2	9.0	3.1	-3.7	29.8	...	16.9	1
(347.3, 40.8).....	2.1	0.6	19.4	-0.6	7.8	...	47.8	-
	-10.5	2.4	7.9	3.1	24.2	...	47.8	1
(353.7, 30.0).....	1.4	0.6	32.8	1.4	8.0	...	12.3	3
	-9.4	15.1	2.8	0.6	39.1	...	12.3	1
	-4.2	2.6	7.2	-10.4	8.3	...	12.3	2
(0.0, 30.0).....	7.1	0.6	48.3	2.4	8.5	...	8.4	-
	-2.3	4.4	10.5	-1.5	23.0	...	8.4	1
(0.6, 24.4).....	9.2	1.6	29.0	3.3	8.2	...	2.8	-
	2.3	3.1	22.3	0.9	18.1	...	2.8	1
(5.1, 34.2).....	3.0	0.9	44.0	0.7	7.9	...	3.1	-
	27.2	17.0	4.3	0.3	29.2	...	3.1	1
(11.3, 25.0).....	2.8	0.4	61.8	2.4	6.7	+10	5.2	-
	8.1	1.4	8.8	-0.1	1.4	+10	5.2	2
	-6.1	6.9	6.9	-0.3	20.7	+10	5.2	1
(36.7, 43.8).....	1.1	0.5	21.7	1.3	5.1	+26	15.8	-
	-6.2	6.2	3.4	-0.7	22.7	+26	15.8	1
(37.3, 33.0).....	-7.8	0.7	23.3	1.4	8.9	-5	16.9	-
	-8.0	19.5	1.8	8.7	36.9	-5	16.9	1

TABLE 2—Continued

(<i>l</i> , <i>b</i>)	<i>B</i>	<i>dB</i>	<i>T_a</i>	<i>V_{LSR}</i>	FWHM	RM	<i>t</i>	Comments
(37.6, 21.4)	4.7	1.0	15.6	2.8	7.1	+30	13.1	–
	–5.6	4.3	7.9	8.6	32.1	+30	13.1	1
	11.2	5.6	2.7	12.7	6.4	+30	13.1	2
(39.0, 43.8)	–2.3	0.6	25.7	–0.7	5.8	+25	8.7	–
	–15.9	5.5	5.2	1.1	17.9	+25	8.7	1
(50.8, 21.4)	0.6	1.0	12.4	3.5	5.7	...	18.6	–
	0.0	1.6	15.8	8.0	22.1	...	18.6	1
	–5.6	3.7	3.4	12.2	5.9	...	18.6	2

NOTE.—In the column headings, *l* is Galactic longitude, *b* Galactic latitude (both in degrees); *B* and *dB* are the line-of-sight magnetic field and its 1 σ error, in microgauss; *T_a* is the antenna temperature of the peak of the Gaussian in kelvins; *V_{LSR}* is the LSR velocity of the Gaussian and FWHM the width of the Gaussian (both in km s^{–1}); RM is the rotation measure from Spoelstra 1971; and *t* is the integration time in hours. Entries in the “Comments” column denote the following: –, considered reliable; 1, considered unreliable because Gaussian is too weak and/or broad; not shown on figures; 2, considered unreliable because Gaussian is too highly blended with other components; not shown on figures; 3, possible narrow structure in *V* spectrum (see § IIc).

neutral H I shell having swept up the ambient magnetic field without producing a large change in its direction.

Heiles *et al.* (1980) used estimates of Faraday depolarization and measurements of H α emission to estimate a lower limit on *B_{||}* of 1.2 μ G in one portion of the NPS; they used observations of the Zeeman effect to place an upper limit of 6 μ G. Our measurements here show that *B_{||}* does indeed rise to ~ 6 μ G in portions of the shell. This supports a shock model for the H I shell. Apparently, the choice of Heiles *et al.* to analyze positions near (*l*, *b*) = (37°, 40°) was simply unfortuitous in terms of actually being able to detect the magnetic field using the Zeeman effect.

Gaussian components shown in Figure 3a typically have $N_{\text{HI}} \approx 2 \times 10^{20}$ cm^{–2}. We have very little idea of the path length along the line of sight, so we cannot estimate a reliable n_{HI} . If the path length is 20 pc, which seems reasonable for a thick shell of this size, $n_{\text{HI}} \sim 4$ cm^{–3}. In a portion of the shell occupied by L204, a filamentary dust cloud, Heiles (1988) estimates $n_{\text{HI}} \sim 9$ –17 cm^{–3}. It seems reasonable that a portion of the shell that contains a dense dark cloud has a higher n_{HI} .

V. THE ERIDANUS REGION

The Eridanus region contains the Eridanus H I shell, a $\sim 38^\circ$ diameter shell expanding at about 23 km s^{–1} (Heiles 1976), and other gas, some of which is unrelated. H I profiles in the Eridanus region usually have more than one distinct peak. One component, with $V_{\text{LSR}} \sim -10$ km s^{–1}, is associated with the approaching side of the Eridanus H I shell. Its receding counterpart, at $\sim +9$ km s^{–1}, is morphologically well defined for $b \lesssim -45^\circ$. Other portions of the region also contain gas at comparable positive velocities, but the shell structure is morphologically less well defined and the gas may not all belong to the Eridanus H I shell. A third velocity component, centered near 0 km s^{–1}, is distributed rather chaotically, and a fourth, centered at about 5 km s^{–1}, appears in part of the region.

We have observed the *V* profile at 10 positions, which yielded a total of 31 well-defined Gaussian components. Figures 4a–4c (Plates 28–30) show the H I column density in three velocity ranges and the corresponding reliable results on *B_{||}*. Table 3 contains all results for *B_{||}* in numerical form.

Figure 4a, which covers the V_{LSR} range -19.2 to -3.2 km s^{–1}, exhibits the approaching portion of the Eridanus shell and shows results on *B_{||}*. There is only one statistically significant

detection, $B_{||} = +3.9 \pm 1.0$ μ G for G211.5–32.8. Two nearby positions have derived fields that are not statistically significant on an individual basis, but taken together have $B_{||} = +2.1 \pm 0.7$ μ G, which is barely significant. We conclude that the portion of the shell near (*l*, *b*) = (211°, -35°) has a positive *B_{||}* of 2–3 μ G. Other portions of the shell have no detected field to 3 σ limits of 2.4–3.3 μ G.

Figure 4b, which covers 6.0–24.0 km s^{–1}, exhibits the receding portion of the Eridanus H I shell, together with other gas centered near +10 km s^{–1}, and shows the results on *B_{||}* both from the present paper and from Troland and Heiles (1982b) for G206.9–49.6. All four positions in the +5 km s^{–1} morphologically prominent portion of the shell at $b \lesssim -45^\circ$ have well-detected field strengths with $B_{||} = -6.7$ to -11.8 μ G. Three of the other positions have +10 km s^{–1} components with large derived *B_{||}*'s of barely acceptable statistical significance. We do not believe the *B_{||}*'s for these three positions, because the peak intensities of these components are very small, less than 4 K. A position near these, G211.5–32.8, has a strong +12.2 km s^{–1} component with $B_{||} = +2.6 \pm 0.9$ μ G, which we regard as a reliable result (but of inadequate statistical significance for a single point). Only the *B_{||}*'s we regard as reliable are shown on Figure 4b, and the only positions where *B_{||}* was detected are in the morphologically well-defined portion of the shell.

For the morphologically well-defined portion of the shell at $b \lesssim -45^\circ$, the H I column densities range from 0.7×10^{20} to 4.3×10^{20} cm^{–2} and *B_{||}* from -11.8 to -6.7 μ G. $|B_{||}|$ increases with decreasing N_{HI} , which is surprising. Troland and Heiles adopt $n_{\text{HI}} = 1.1$ cm^{–3} for G206.9–49.6, the position having the largest N_{HI} . This volume density is probably too low, because the structure appears to be a filament instead of an edge-on shell. If the filament is circular in cross section, then at its probable distance of 450 pc (Reynolds and Ogden 1979) its angular diameter of $\sim 3^\circ$ implies a linear diameter of 24 pc and $n_{\text{HI}} \approx 5.8$ cm^{–3}. The volume densities for G195.4–50.2 and G199.0–50.2 are probably comparable, because, although the column densities are smaller, the filament looks thinner at these positions. The volume density for G191.5–50.5 may be smaller both because the column density is 2.4 times smaller and because the structure looks larger at this position.

Figure 4c covers the central V_{LSR} range, -2.0 to $+9.0$ km

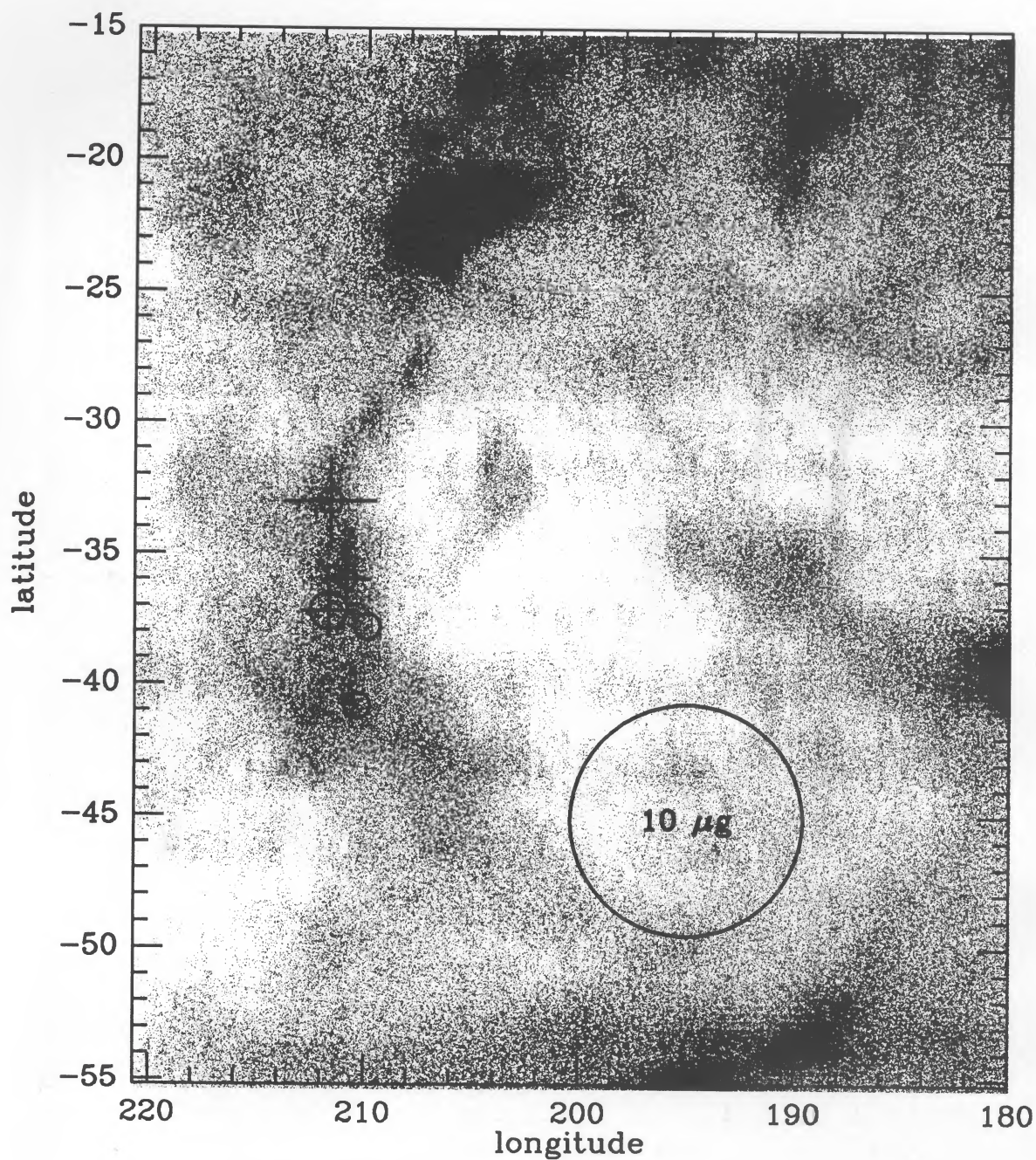


FIG. 4a

FIG. 4.—(a) Map of the Eridanus region, showing N_{HI} between -19.2 and -3.2 km s^{-1} and derived B_{\parallel} 's from Table 3. Plus signs indicate positive B_{\parallel} , crosses indicate negative B_{\parallel} , with size proportional to the value; circles indicate the 1σ error. Higher quality H I maps can be found in Colomb, Pöppel, and Heiles (1980) and Heiles (1984a). (b) Map of the Eridanus region, showing N_{HI} between 6.0 and 24.0 km s^{-1} and derived B_{\parallel} 's from Table 3. Plus sign indicates positive B_{\parallel} , crosses indicate negative B_{\parallel} , with size proportional to the value; circles indicate the 1σ error. Higher quality H I maps can be found in Colomb, Pöppel, and Heiles (1980) and Heiles (1984a). (c) Map of the Eridanus region, showing N_{HI} between -2.2 and 6.0 km s^{-1} and derived B_{\parallel} 's from Table 3. Plus signs indicate positive B_{\parallel} , cross indicates negative B_{\parallel} , with size proportional to the value; circles indicate the 1σ error. Higher quality H I maps can be found in Colomb, Pöppel, and Heiles (1980) and Heiles (1984a).

HEILES (see 336, 815)

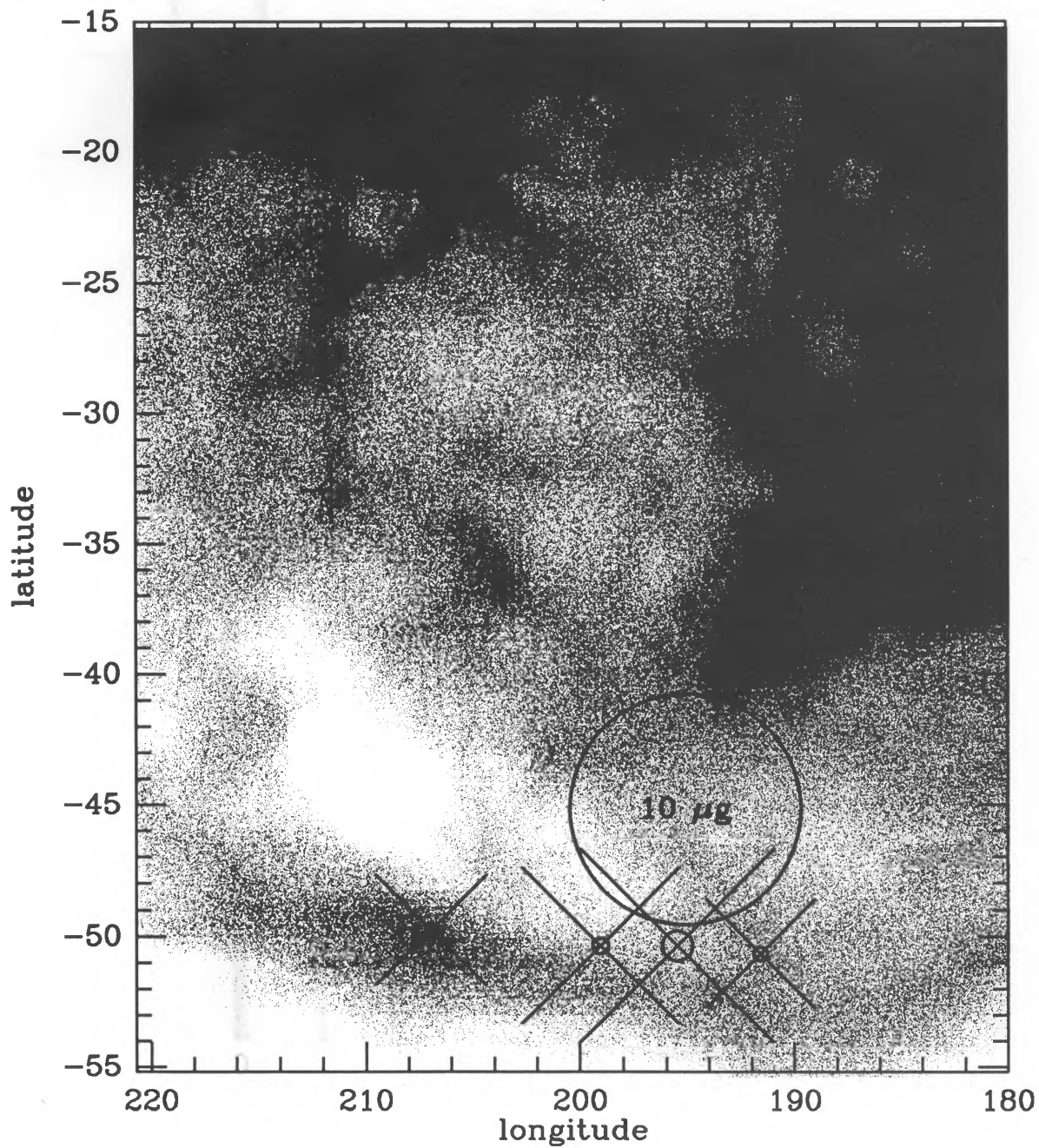


FIG. 4b

HEILES (see 336, 815)

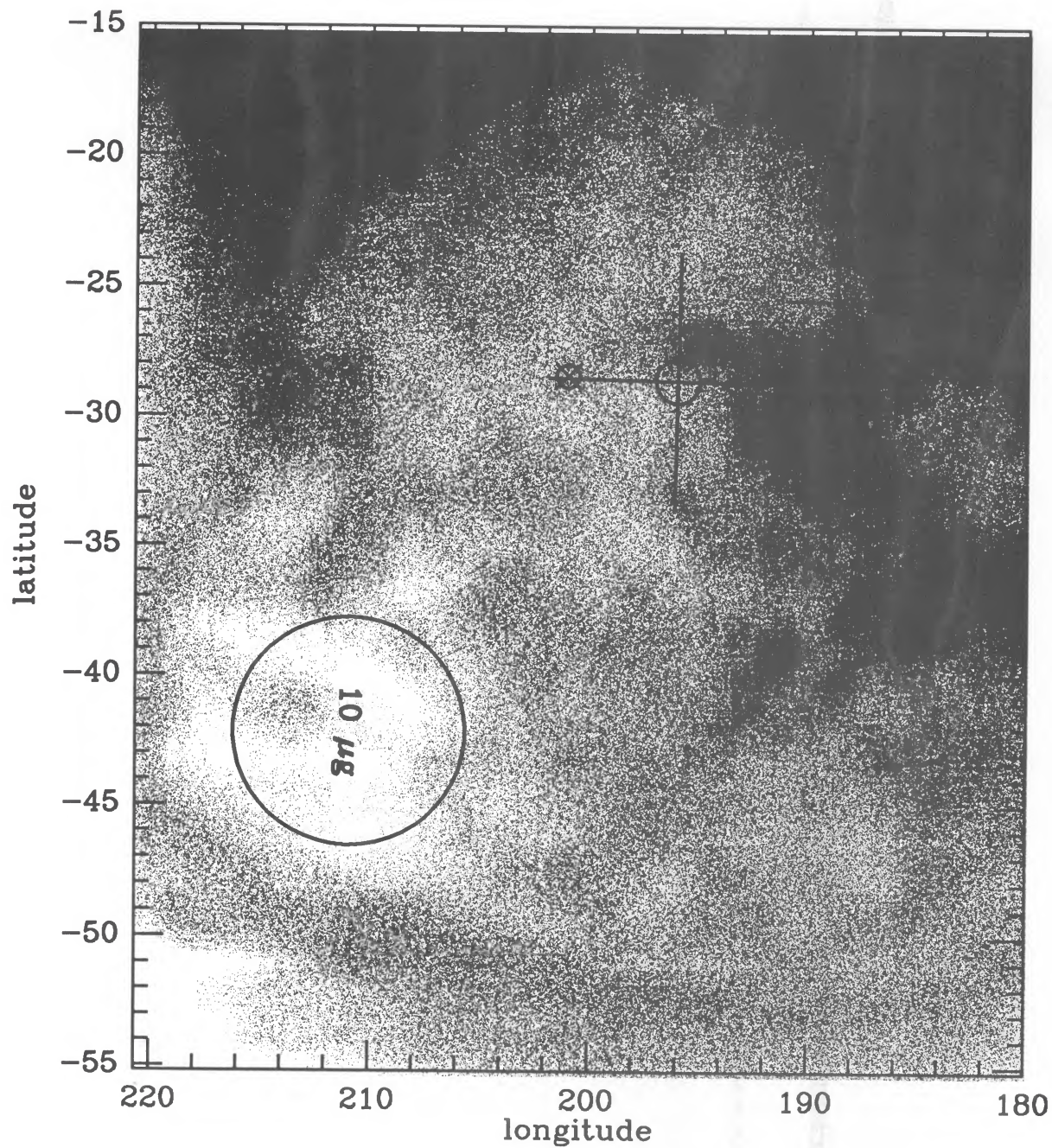


FIG. 4c

HEILES (see 336, 815)

HEILES

 TABLE 3
 GAUSSIAN COMPONENTS FOR THE ERIDANUS SHELL

(l, b)	B	dB	T_a	V_{LSR}	FWHM	t	Comments
(191.5, -50.5).....	-6.6	0.6	18.7	7.7	4.8	52.5	-
	-0.7	3.5	6.8	3.8	22.2	52.5	1
(195.4, -50.2).....	-11.8	1.3	9.3	6.9	4.0	11.6	-
	-5.4	1.9	7.7	-0.9	5.2	11.6	2
	29.8	5.2	5.5	1.9	21.2	11.6	1
(199.0, -50.2).....	-9.5	0.7	18.5	5.9	3.7	10.9	-
	29.5	8.3	4.0	4.7	21.6	10.9	1
(204.4, -21.4).....	0.1	0.8	27.0	-8.4	6.5	16.7	-
	-4.5	1.7	15.6	8.1	5.7	16.7	2
	-2.7	1.1	26.2	14.5	8.3	16.7	-
	-5.2	1.8	15.0	2.3	6.9	16.7	2
(209.8, -37.6).....	0.0	1.1	13.1	-9.4	4.5	22.4	-
	-11.2	6.9	1.3	0.9	1.9	22.4	1
	-15.9	5.3	3.9	10.2	9.6	22.4	1
	44.2	13.0	3.4	-2.4	38.7	22.4	1
(210.3, -40.6).....	0.1	1.1	12.4	-9.5	6.3	29.4	-
	29.5	12.1	2.7	-1.6	32.6	29.4	1
(210.8, -35.8).....	2.1	0.8	15.1	-10.0	5.2	37.4	-
	0.0	0.5	19.7	1.2	2.7	37.4	3
	14.9	4.4	3.7	15.7	8.3	37.4	1
	35.9	8.0	3.9	-0.6	29.3	37.4	1
(211.5, -32.8).....	3.9	1.0	13.5	-7.8	4.6	33.4	-
	11.2	1.9	7.6	4.6	5.0	33.4	-
	2.6	0.9	17.6	12.2	5.9	33.4	-
	17.0	5.8	6.0	4.4	31.9	33.4	1
(211.6, -37.0).....	2.3	1.6	8.5	-12.9	6.3	36.1	-
	-1.5	1.0	9.8	0.8	3.0	36.1	-
	36.0	11.6	3.4	4.7	44.3	36.1	1
	15.8	6.6	2.4	13.9	7.9	36.1	1
(215.4, -26.8).....	4.3	0.3	35.9	6.4	4.9	17.7	-
	9.5	2.3	7.8	6.3	15.4	17.7	1

NOTE.—In the column headings, l is Galactic longitude, b Galactic latitude (both in degrees); B and dB are the line-of-sight magnetic field and its 1σ error, in microgauss; T_a is the antenna temperature of the peak of the Gaussian in kelvins; V_{LSR} is the LSR velocity of the Gaussian and FWHM the width of the Gaussian (both in km s^{-1}); t is the integration time in hours. Entries in the “Comments” column denote the following: -, considered reliable; 1, considered unreliable because Gaussian is too weak and/or broad; not shown on figures; 2, considered unreliable because Gaussian is too highly blended with other components; not shown on figures; 3, possible narrow structure in V spectrum (see § IIc).

s^{-1} , and shows the determinations of B_{\parallel} we consider reliable for components centered within this range. Most of the components are excluded from the figure because they are either too weak or too broad to provide reliable fits for B_{\parallel} . Two of the positions, G211.5–32.8 and G215.4–26.8, show statistically significant fields of $+11.2 \pm 1.9$ and $+4.3 \pm 0.3 \mu\text{G}$, respectively. These components, with V_{LSR} 's of 4.6 and 6.4 km s^{-1} , respectively, differ in velocity from the $\approx 1 \text{ km s}^{-1}$ components of the two nearby positions G210.8–35.8 and G211.6–37.0, both of which show statistically undetected B_{\parallel} 's of less than a few microgauss. The G211.5–32.8 and G215–26.8 components appear to be part of a different shell structure, which has a positive B_{\parallel} .

VI. REGION A OF SIMARD-NORMANDIN AND KRONBERG (1980)

Region A occupies a bit more than 1 sr at negative latitudes for $l \sim 80^\circ$ – 130° . Extragalactic radio sources in this region have large negative RMs, corresponding to positive fields. The large RMs suggest that B_{\parallel} might be systematically high and easily detectable. We chose 22 positions in this region, mostly toward radio sources for which RMs were determined by Simard-Normandin, Kronberg, and Button (1981); the results

are presented numerically in Table 4, together with the RMs for the sources and, where available, RMs determined from the diffuse Galactic synchrotron radiation by Spoelstra (1972).

a) The H I Shell GS 058–10+4

Being centered at $b \approx -10^\circ$, this $\sim 12^\circ$ diameter straddles the $|b| = 10^\circ$ latitude border between “Galactic plane” and “high latitude” H I surveys, and is therefore not easily visible in either; see Figure 1n of the presentation of merged data sets of Heiles (1984a). Two of our positions, G64.2–10.6 and G64.4–10.8, lie on this shell. These positions are very close together. Each has a weak Gaussian component centered near 4.0 km s^{-1} ; the derived field strengths are $+9.9 \pm 1.9$ and $+6.9 \pm 2.5 \mu\text{G}$, respectively, although they are somewhat unreliable because of blending (see Fig. 1c). The two derived B_{\parallel} 's agree within the errors, and it is reasonable to adopt the average, 8.4 μG .

b) GS 062–23+13

Only a portion of this shell is bright and distinct; see Figure 1o of Heiles (1984a). The shell appears as a 90° sector of a circular arc running from $(l, b) \approx (60^\circ, -10^\circ)$ to $(42^\circ, -26^\circ)$.

TABLE 4
GAUSSIAN COMPONENTS FOR REGION A

(l, b)	B	dB	T_a	V_{LSR}	FWHM	RM	t	Comments
(43.5, -22.6).....	0.3	1.0	11.8	1.6	7.2	...	23.6	-
	7.1	0.7	16.1	13.2	5.0	...	23.6	-
	-4.7	0.7	14.1	18.4	4.2	...	23.6	1
	15.8	2.2	9.5	9.7	23.1	...	23.6	2
(51.5, -14.8).....	3.8	1.0	28.8	14.4	7.1	(2019+09: -117)	5.5	-
	6.6	2.3	15.6	3.8	11.2	(2019+09: -117)	5.5	-
(56.7, -40.6).....	-0.7	3.2	21.0	6.3	7.2	(2154-016: +1)	0.9	-
	-1.2	2.3	25.9	-4.5	5.7	(2154-016: +1)	0.9	-
(62.2, -10.6).....	4.3	0.6	24.2	13.5	6.4	...	18.4	-
	1.0	2.5	10.7	12.6	24.8	...	18.4	2
(64.2, -10.6).....	0.3	1.6	14.4	15.3	16.1	...	30.6	3
	9.9	1.9	7.4	4.0	6.4	...	30.6	-
	15.4	31.5	1.8	-1.1	102.4	...	30.6	2
(64.4, -10.8).....	22.1	2.3	11.9	15.3	21.5	(2031+31: -148)	28.5	1
	6.9	2.5	5.6	4.2	5.4	(2031+31: -148)	28.5	1
(80.2, -18.8).....	2.8	2.5	5.6	2.9	9.1	(2141+27: -53)	17.0	-
	-13.4	3.7	6.9	-3.0	29.8	(2141+27: -53)	17.0	2
(84.9, -20.9).....	-0.2	1.7	12.8	3.7	8.1	(2203+29: -125)	5.5	-
	-59.3	7.9	5.5	-9.1	30.7	(2203+29: -125)	5.5	2
(92.6, -31.4).....	2.9	3.6	15.4	-5.4	5.1	(2251+24: -558)	2.8	-
	12.7	15.7	7.0	-3.7	19.7	(2251+24: -558)	2.8	2
(93.1, -47.1).....	-3.4	2.4	15.1	-3.9	13.7	(2328+10: -307)	2.7	-
(96.8, -19.6).....	8.4	0.5	15.6	1.1	3.4	(2244+36: -231)	43.2	-
	4.1	1.5	6.1	-22.3	6.2	(2244+36: -231)	43.2	-
	18.3	1.0	15.0	3.5	13.4	(2244+36: -231)	43.2	1, 2
	-3.3	3.2	6.3	-14.0	26.6	(2244+36: -231)	43.2	2
(98.1, -17.1).....	-1.7	1.3	15.5	-0.9	17.0	(2243+39: -275)	16.6	-
	-8.4	2.2	7.5	-25.0	11.9	(2243+39: -275)	16.6	-
(99.7, -31.2).....	1.2	1.5	13.1	-4.1	12.3	(2319+27: -254)	9.8	-
	66.1	29.7	1.5	-15.9	66.7	(2319+27: -254)	9.8	2
(102.8, -41.7).....	-4.0	2.0	14.8	-4.9	11.0	(2345+18: -55)	2.7	-
(103.5, -33.1).....	8.2	3.2	12.6	-1.1	15.5	(2335+26: +102)	2.7	-
(113.7, -12.0).....	-3.1	1.2	18.8	-1.6	14.1	+1; (2353+49: -182)	10.1	-
	-12.1	4.9	5.8	-19.3	21.0	+1; (2353+49: -182)	10.1	2
	50.5	33.1	1.5	-27.4	80.4	+1; (2353+49: -182)	10.1	2
(134.2, -38.4).....	0.8	0.4	24.0	-3.4	10.3	+1; (0127+23: -65)	26.1	-
(137.3, -51.6).....	1.3	2.7	16.0	-9.6	5.6	(0124+09: -4)	3.7	-
	4.3	4.5	14.2	-7.8	12.3	(0124+09: -4)	3.7	2
(141.2, -16.6).....	-7.8	1.7	9.5	2.0	9.0	0; (0219+42: -67)	12.2	-
	58.2	12.5	2.5	-37.8	31.6	0; (0219+42: -67)	12.2	2
	-20.1	5.0	5.8	-4.1	23.7	0; (0219+42: -67)	12.2	2
(145.6, -24.0).....	3.4	0.9	18.2	0.3	7.5	0; (0229+34: -63)	6.7	-
	75.9	17.8	2.1	-6.0	35.9	0; (0229+34: -63)	6.7	2
(147.3, -26.4).....	-3.3	0.8	21.4	1.8	4.3	0; (0231+31: +16)	14.1	-
	-1.6	2.8	7.2	-4.0	5.5	0; (0231+31: +16)	14.1	1
	5.3	2.8	11.4	-0.6	14.6	0; (0231+31: +16)	14.1	2
(150.6, -27.3).....	-1.3	0.9	11.8	-5.4	4.1	0; (0241+29: -60)	22.1	1
	2.6	1.0	17.8	-0.3	5.9	0; (0241+29: -60)	22.1	3
	-2.6	0.7	14.6	4.2	3.5	0; (0241+29: -60)	22.1	1
	7.3	2.3	11.2	0.1	15.1	0; (0241+29: -60)	22.1	2

NOTE.—In the column headings, l is Galactic longitude, b Galactic latitude (both in degrees); B and dB are the line-of-sight magnetic field and its 1σ error, in microgauss; T_a is the antenna temperature of the peak of the Gaussian in kelvins; V_{LSR} is the LSR velocity of the Gaussian, FWHM the width of the Gaussian (both in km s^{-1}); RM is the rotation measure (RMs not in parentheses from Spoelstra 1972; RMs in parentheses are for the listed extragalactic radio source, from Simard-Normandin, Kronberg, and Butten 1981); and t is the integration time in hours. Entries in the "Comments" column denote the following: -, considered reliable; 1, considered unreliable because Gaussian is too highly blended with other components; not shown on figures; 2, considered unreliable because Gaussian is too weak and/or broad; not shown on figures; 3, possible narrow structure in V spectrum (see § IIc).

Three of our positions, G43.5–22.6, G51.5–14.8, and G62.2–10.6, lie on this arc. These three positions have Gaussian components centered near 14 km s^{-1} with well-determined B_{\parallel} 's of 7.1 ± 0.7 , 4.3 ± 0.6 , and $3.8 \pm 1.0 \mu\text{G}$, respectively. Two other nearby positions, G64.2–10.6 and G64.4–10.8, do not lie on the arc. The derived results are shown with an H I map on Figure 5 (Plate 31).

N_{HI} for the three positions averages $\sim 2.9 \times 10^{20} \text{ cm}^{-2}$. The shell thickness is about $1^{\circ}5$. At these low latitudes the shell is not necessarily nearby, and its V_{LSR} of $\sim 13 \text{ km s}^{-1}$ might result from Galactic rotation (but hardly necessarily so; see GS 092–29–23 below). If so, the distance is $\sim 900 \text{ pc}$. If the shell is a filament, circular in cross section, the path length along the line of sight is $\sim 23 \text{ pc}$ and $n_{\text{HI}} \sim 4.1 \text{ cm}^{-3}$.

c) GS 092–29–23

This shell is an irregular closed elliptical H I filament. Two of our positions lie on this filament, G96.8–19.6 and G98.1–17.1. These positions have weak Gaussian components centered near -23 km s^{-1} with $B_{\parallel} = +4.1 \pm 1.5$ and $-8.4 \pm 2.2 \mu\text{G}$, respectively. Only the latter result has formal statistical significance, and then only barely so. The spectra and fit for G96.8–19.6 are shown above in Figure 1*b*; the V spectrum for G98.1–17.1 is noisier. Neither fit instills much confidence to the eye. The derived B_{\parallel} 's and H I map are shown on Figure 6 (Plate 32). N_{HI} averages $1.1 \times 10^{20} \text{ cm}^{-2}$ for these two positions. If the filament width is $1^{\circ}5$ and the distance 200 pc , then $n_{\text{HI}} \approx 7 \text{ cm}^{-3}$.

d) The “Radio Loop II” H I Shell

This shell runs parallel to and lies inside of radio Loop II; it is easily visible in the Colomb, Pöppel, and Heiles (1980) maps at -8 and -13 km s^{-1} . It is not known whether the association with Loop II is real. Two of our positions lie in the shell, G134.2–38.2 and G137.3–51.6. They have derived B_{\parallel} 's of $+1.3 \pm 2.7$ and $+8.4 \pm 2.1 \mu\text{G}$, respectively. Troland and Heiles (1982*a*) measured $B_{\parallel} = -6.9 \pm 1.2$ for G156.8–49.3. We conclude that this shell has magnetic field structure on angular scales $\lesssim 12^{\circ}$.

e) The Other Positions

The results for all positions, except for the Gaussian components for the positions shown above, are shown superposed on a map of H I column density in Figure 7 (Plate 33). There are only a few results having individual statistical significance. There does not seem to be any systematic pattern to either the sign or the strength of B_{\parallel} . In contrast, the RMs of extragalactic sources in this region are almost uniformly strong and negative. Thus, there is no discernible correlation of B_{\parallel} with RM. Specifically, there are eight positions in Table 4 having both statistically significant Zeeman-derived B_{\parallel} 's and extragalactic RMs; of these, the two fields are parallel for five positions and antiparallel for three.

Heiles (1984*b*) used the RMs and EMs derived from H α emission to estimate B_{\parallel} and n_e in the magnetoactive region. The values depend on the assumed length along the line of sight over which the magnetoactive region extends. Heiles argued that a length of $\sim 1 \text{ kpc}$ is reasonable; this provides $n_e \approx 0.1 \text{ cm}^{-3}$ and $B_{\parallel} \approx 2.5 \mu\text{G}$. Such a low field strength is compatible with the low and/or indeterminate values obtained from our Zeeman effect measurements. Smaller choices for

path length lead to localized regions of higher n_e and B_{\parallel} . In either case, the neutral H I would occupy different regions of space and we would not necessarily expect a strong correlation between RM and B_{\parallel} .

Although H I shell structure does appear on Figure 7, the shells seem morphologically less well defined than in the other figures. Thus the data in Figure 7 serve as a crude comparison with data presented in most of the other figures, which cover morphologically well-defined shells. However, it is not a true “control region,” because shell structure does appear on Figure 7 and the definition of “morphologically well defined” is a subjective one. The average $\langle |B_{\parallel}| \rangle$ for all data in Figure 7 is $3.4 \mu\text{G}$, with a standard deviation of $2.6 \mu\text{G}$. If we had a true control region in which shells were really absent, $\langle |B_{\parallel}| \rangle$ would probably be even smaller. In any case, $|B_{\parallel}|$ for these positions is smaller than typical $|B_{\parallel}|$'s for the well-defined shells.

VII. GAUSSIAN DECOMPOSITION AND THE
“WARM NEUTRAL MEDIUM”

In their comprehensive review of the interstellar medium, KH discuss the phases of the interstellar gas. Two phases are neutral: the cold neutral medium (CNM) and the warm neutral medium (WNM). KH discuss the available data in terms of contemporary theory, under the assumption that all the WNM has the same temperature. They find that the most reasonable value for the WNM temperature is $\sim 8000 \text{ K}$.

Our Gaussian decompositions show that this temperature is too high in some regions. For single-peaked profiles, our fits of one narrow and one broad Gaussian are usually very good, leaving very small residuals. H I at 8000 K has a thermal FWHM of 19.2 km s^{-1} , and many of our broad Gaussians are not this wide. For example, in Table 1, only three of the 12 positions have FWHM $> 19.2 \text{ km s}^{-1}$; the minimum FWHM (G135.3+40.8) corresponds to $T < 1930 \text{ K}$. Observationally similar conclusions have been obtained in some regions by Verschuur and Schmelz (1988).

Such narrow FWHMs for the broad components are unusual. Mebold (1972) decomposed about 1300 H I line profiles into Gaussians and found the mean FWHM of the broad components to be about 20.7 km s^{-1} . One might suspect that the disagreement results from inaccurate data or from the fact that Gaussians do not form an orthogonal set of functions with which to fit uniquely an H I profile. In fact, however, neither possibility applies. Mebold presents his profile for the position $(l, b) = (125^{\circ}7, 31^{\circ}9)$, which is only $0^{\circ}44$ away from one of our NCP positions. Both his data and his Gaussian decomposition agree very well with ours. Indeed, this agreement is very much expected, because the technology of 21 cm spectroscopy was highly developed in the late 1960s, when Mebold's data were obtained; furthermore, the FWHMs of the narrow and wide components differ enough, and single-peaked profiles are simple enough, so that the lack of uniqueness of Gaussian decomposition is not a problem in practice.

We conclude that the WNM is *not* all at the same temperature. Our observations are, in the main, directed toward morphologically prominent H I shells. We conclude that the WNM associated with these shells is commonly much cooler than 8000 K . Casual perusal of our tables shows that other positions, probably not associated with morphologically prominent H I shells, also have “too cool” WNM; this point needs detailed investigation, which is beyond the scope of the present paper.

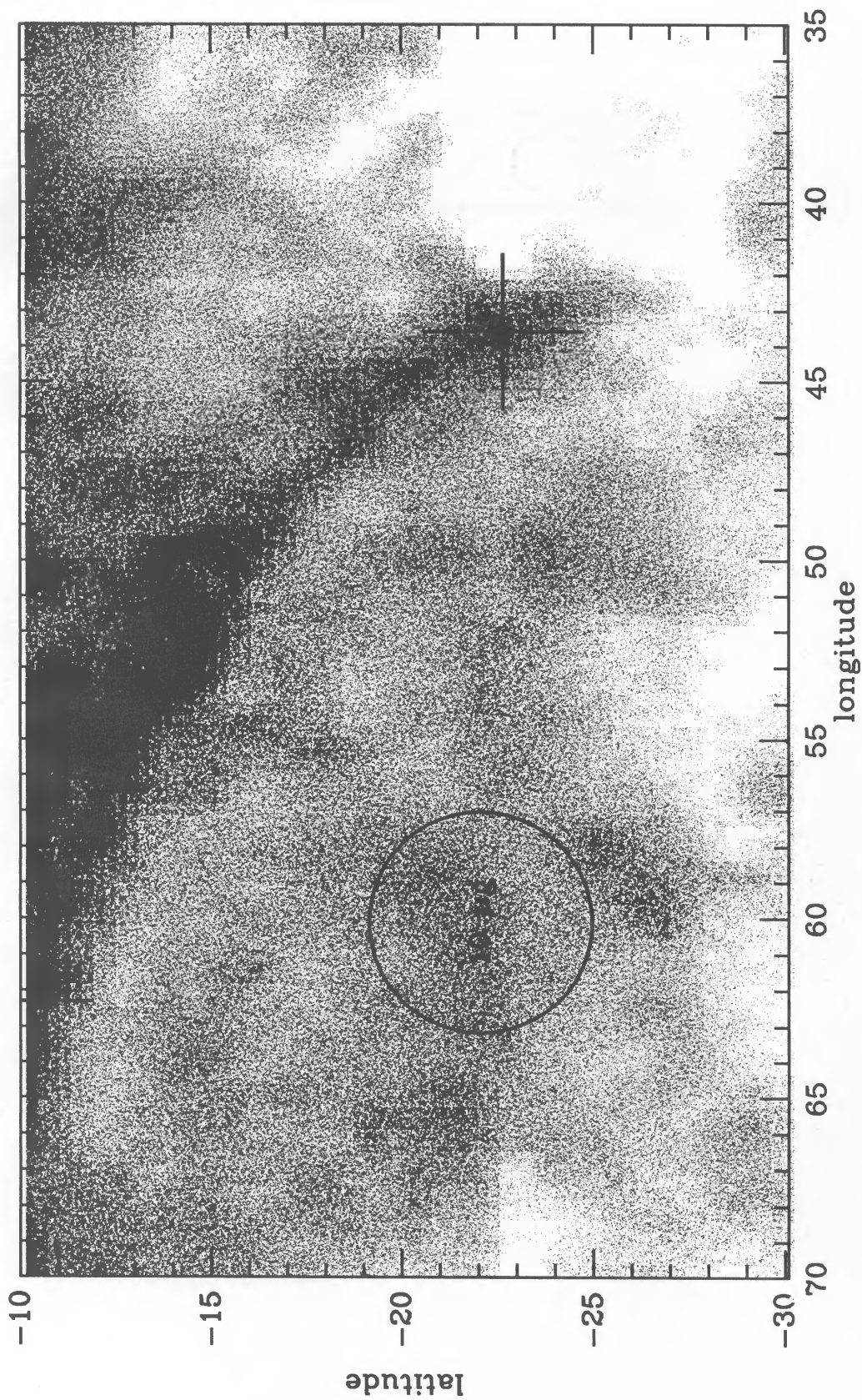


FIG. 5.—Map of GS 062—23+13, showing N_{HI} between 11.0 and 19.0 km s^{-1} and derived B_{\parallel} 's from Table 4. Plus signs indicate positive B_{\parallel} ; circles indicate the 1σ error. Higher quality H I maps can be found in Colomb, Pöppel, and Heiles (1980) and Heiles (1984a).

HEILES (see 336, 818)

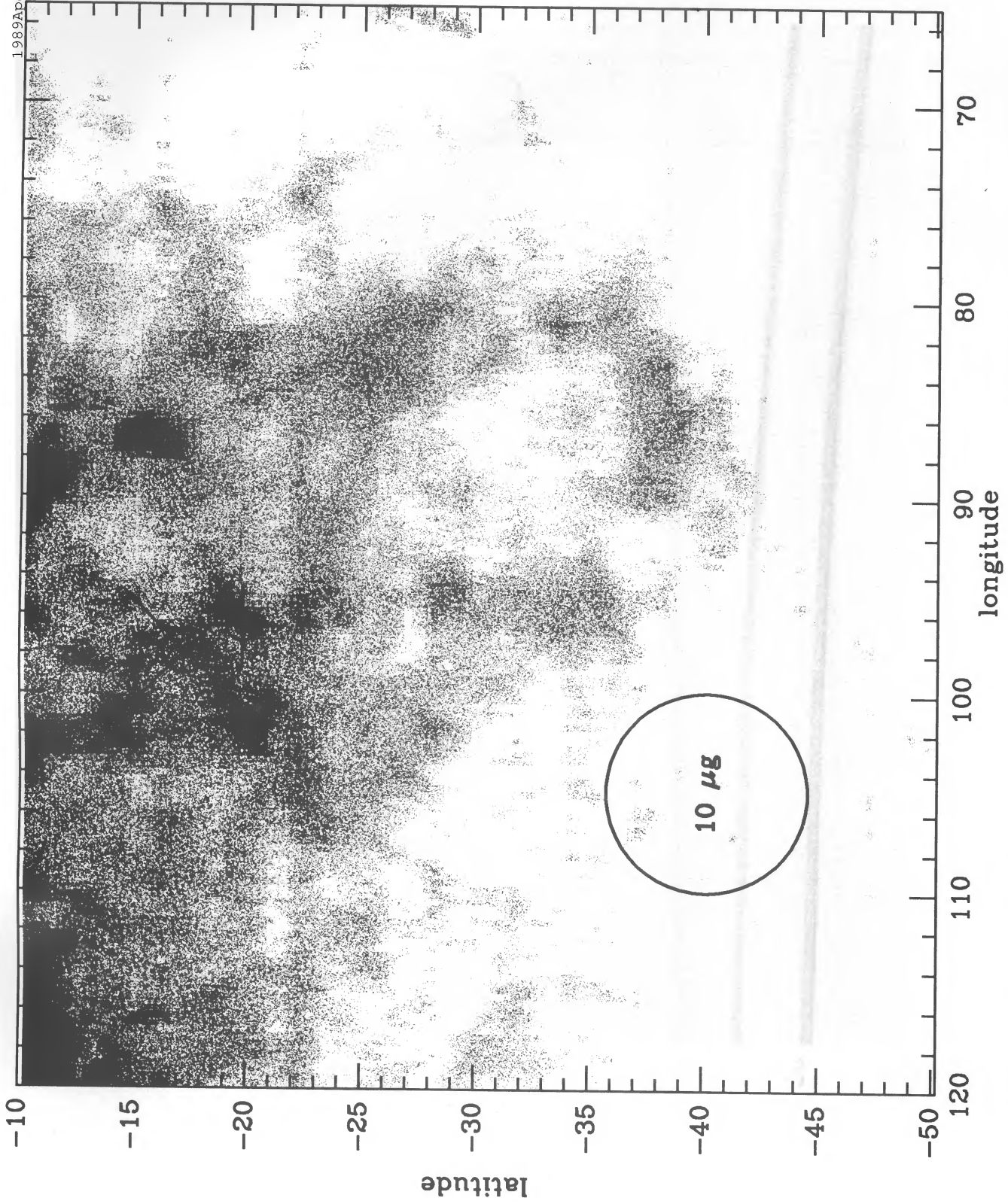


FIG. 6.—Map of GS 092-29-23, showing $N_{\text{H I}}$ between -16.1 and -28.5 km s^{-1} and derived B_{\parallel} 's from Table 4. Plus sign indicates positive B_{\parallel} , cross indicates negative B_{\parallel} , with size proportional to the value; circles indicate the 1σ error. Higher quality H I maps can be found in Colomb, Pöppel, and Heiles (1980) and Heiles (1984a).

HEILES (see 336, 818)

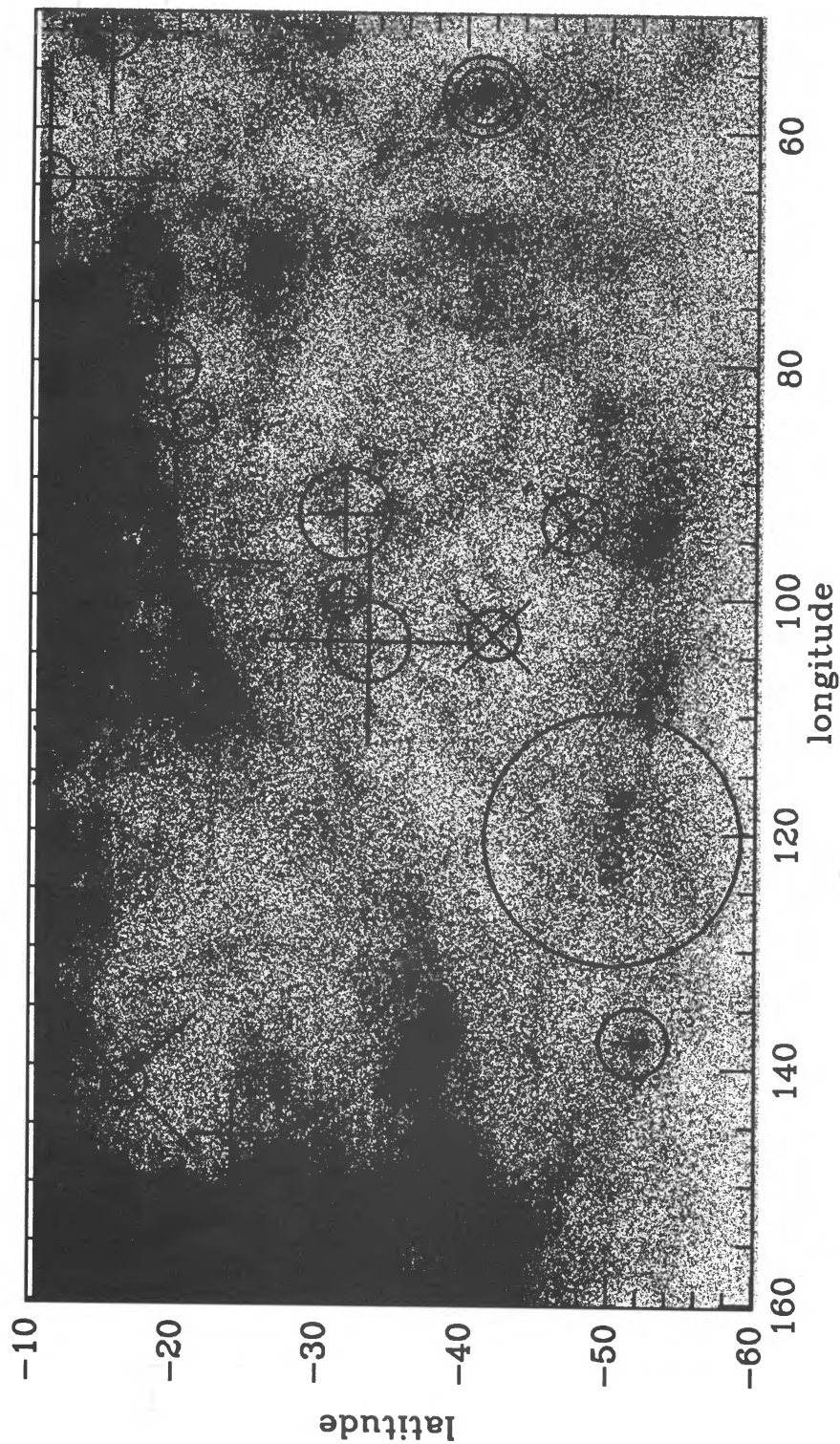


FIG. 7.—Map of region A of Simard-Normandin and Kronberg (1980), showing $N_{\text{H II}}$ between -12.0 and $+12.0 \text{ km s}^{-1}$ and derived B_{\parallel} 's from Table 4. Plus signs indicate positive B_{\parallel} ; crosses indicate negative B_{\parallel} , with size proportional to the value; circles indicate the 1σ error.

HEILES (see 336, 818)

VIII. DISCUSSION

a) *Interstellar Pressure*

As a general tendency, we often find easily detectable fields in H I shell structures. We consider five shells as morphologically well defined: the NCP shell; the NPS shell; the $b \lesssim -45^\circ$ portion of the Eridanus shell; GS 058-10+4; and GS 062-23+13. Values of $\langle |B_{\parallel}| \rangle$ for these shells are 5.8, 4.0, 8.7, 8.4, and 5.1 μG , respectively. This leads to a grand average over the five shells of $\langle |B_{\parallel}| \rangle \approx 6.4 \mu\text{G}$. Including a factor of 2 to relate $\langle |B_{\parallel}| \rangle$ to $\langle |B| \rangle$, this corresponds to a magnetic pressure $P_{\text{mag}} = B^2/8\pi \approx 6.5 \times 10^{-12} \text{ ergs cm}^{-3}$ or $\approx 4.7 \times 10^4 \text{ cm}^{-3} \text{ K}$.

We typically derive $n_{\text{HI}} \sim 7 \text{ cm}^{-3}$ in these structures. This is very uncertain, because it depends on assuming that the H I structures are filaments of circular cross section; on assuming a distance; and on assuming there is no small scale clumping. If the structures are edge-on sheets instead of filaments, our derived n_{HI} values are too large; if there is small-scale clumping, they are too small.

The gas pressure is not easily measurable, because the gas temperature cannot be obtained without a measurement of the H I line in absorption against a background continuum source. Some sparse information exists for some of the structures discussed in this paper. The Eridanus H I probably has measured temperatures ranging from 55 to $>600 \text{ K}$; the NPS H I has temperatures of order 100 K; one position in the NCP shell has $T \approx 316 \text{ K}$, but this position is not in the dense portion of the filament. If we adopt a temperature of 100 K for illustration, the value of n_{HI} gives $P_{\text{gas}} \approx 700 \text{ cm}^{-3} \text{ K}$. This is 67 times smaller than P_{mag} .

H I line widths are universally larger than thermal, which leads to a significant "turbulent" pressure P_{turb} . This is a long-established observational fact, and is also easily seen from the tables of Gaussian parameters presented in this paper. The narrow Gaussian components typically have FWHM $\sim 5.5 \text{ km s}^{-1}$. If this were purely thermal, it would correspond to a FWHM-derived temperature of 660 K. This corresponds to $P_{\text{turb}} \approx 4600 \text{ cm}^{-3} \text{ K}$, close to the commonly accepted standard interstellar pressure (KH). P_{turb} is ~ 10.3 times smaller than P_{mag} .

We conclude that P_{mag} dominates both P_{gas} and P_{turb} in H I shells and filaments. This is the same conclusion reached earlier by Troland and Heiles (1982*b*), who discussed the results for one position in the Eridanus H I shell. They went on to interpret the situation in terms of an isothermal shock, which should be roughly applicable even if the ambient gas was not cool H I, because the postshock region is dominated by cooled gas.

$P_{\text{mag}} \sim 4.7 \times 10^4 \text{ cm}^{-3} \text{ K}$ within in the H I structures, much larger than the standard thermal pressure adopted for interstellar space. This leads one to expect that these structures should be undergoing rapid expansion. However, gas moves in reaction to pressure *gradients*, so the large P_{mag} will induce motions only if P_{mag} decreases outside the structure. We cannot reliably measure B_{\parallel} outside the structure. If the large B_{\parallel} 's we have derived for some broad Gaussian components are real, which is probably not the case, and if the broad Gaussian components refer to gas lying in the warmer, less dense regions in the outer portions of a structure, which is probably the case, then the magnetic pressure gradient may indeed be small.

Furthermore, it is the *total* pressure gradient that is important. H I shells are produced by the overpressure of the hot

ionized medium (HIM), which in turn is heated by stellar winds and supernovae. The total pressure in a shell should be closely comparable to the total pressure of the adjacent HIM that produces the shell. Thus, typical HIM pressures associated with our shells should be $\sim 5 \times 10^4 \text{ cm}^{-3} \text{ K}$.

b) *Nonthermal Line Widths*

Alfvén velocities V_A are comparable to H I line widths. With $B \approx 12.8 \mu\text{G}$ and $n_{\text{HI}} \approx 7 \text{ cm}^{-3}$, $V_A \approx 9.7 \text{ km s}^{-1}$. This is about 1.8 times larger than the typical line width. This suggests that line widths, which are nearly always supersonic, are not necessarily super-Alfvénic—and that line widths may actually be limited by, or closely related to, the Alfvén velocity. This is not a particularly new idea (Arons and Max 1975; Zweibel and Josafatsson 1983; Elmegreen 1985; Falgarone and Puget 1986; Shu, Adams, and Lizano 1987; Myers and Goodman 1988). It has the interesting corollary that the Zeeman effect should be more easily detected in broad than in narrow lines. Historically, narrow lines were preferred, and the attempts to discover interstellar Zeeman splitting were concentrated on the narrow H I absorption line of Cas A, which turned out to be a mistake and delayed the discovery by several years (see Verschuur 1969).

c) *Thermally Unstable Gas*

In § VII we found wide Gaussian components having FWHMs that limit the temperature to $<2000 \text{ K}$ in some regions. As stressed by KH, temperatures in this range are thermally unstable in pressure equilibrium. For $nT = 3000 \text{ cm}^{-3} \text{ K}$, the cooling time scale is $\sim 1.0 \times 10^6 \text{ yr}$ for $T = 2000 \text{ K}$ (KH). Many of these wide Gaussians apply to gas that was part of expanding shells. For typical supernova-produced shells, it takes longer than 10^6 yr for the shell to stop expanding. Thus the cooling time scale is shorter than the time scale associated with the shell dynamics, and the thermally unstable state should not be attributable to shell dynamics. If "too cool" WNM also exists outside well-defined shells, as we suspect, then we could in no way ascribe the thermally unstable state to shell dynamics.

The thermally unstable state is not modified by uniform magnetic fields. In his classic paper, Field (1965) showed that a uniform magnetic field has no appreciable effect on thermal instability because the gas can move freely parallel to the field lines. It remains to investigate the possible effect of the nonuniform field caused by Alfvén waves, which, as discussed above, probably produce an appreciable fraction of the line width of narrow components. The shortest wavelength over which thermal instability occurs is limited by thermal conduction, and is $\sim 6 \times 10^{15} n_{\text{HI}}^{-1} \text{ cm}$. The shortest Alfvén wavelength is limited by ion-neutral damping (Zweibel and Josafatsson 1983), and is $\sim 6 \times 10^{17} n_{\text{HI}}^{-3/2} \text{ cm}$, which for reasonable parameters is much larger than the limiting wavelength for thermal instability. Thus thermal conductivity cannot affect thermal instability in Alfvén waves.

Cox (1987) has postulated that the magnetic field may suppress thermal instability by forcing the gas to evolve at constant gas density instead of constant gas pressure. Presumably, this can occur only in a strong, nonuniform field; the details remain to be explored. In this case, the equilibrium temperature can be stable over a wide range of values, and might allow the "too cool" gas to exist in stable equilibrium.

The "too cool" WNM, in thermally unstable pressure equilibrium, may exist not only in prominent H I shells. This situ-

ation cries out for further investigation. Parts of the task are straightforward, requiring only the fitting of Gaussian components to a large sample of H I profiles; the data do not require correction for "stray radiation" because the *absence* of wide WNM wings is the issue of importance. However, the interpretation is not straightforward, because the average FWHM has been well established to be about 20.7 km s^{-1} for a reasonably large and apparently unbiased sample of profiles (Mebold 1972).

d) B in H I versus B in Less Dense Regions

In the discussions above we noted that our Zeeman-derived B_{\parallel} 's do not correlate with values obtained from Faraday rotation. This is also the case toward Tau A, for which the two methods yield oppositely directed B_{\parallel} 's (Heiles 1987). Also, in the North Polar Spur the magnetic field in H I differs from that in adjacent less-dense regions: the transverse component of B derived from the optical polarization is much different from that derived from the polarization of diffuse synchrotron emission (Spoelstra 1971).

The absence of correlation is not unreasonable, because the various techniques sample different kinds of region, in which the magnetic field plays different roles. H I Zeeman splitting samples H I clouds, while Faraday rotation samples the warm ionized medium (WIM) that is responsible for pulsar dispersion and H α emission (Heiles 1987); the WIM is fully ionized. Comparison of pulsar RM and DM implies that B in the WIM is dominated by the random component and is equal to about $5 \mu\text{G}$ (Rand and Kulkarni 1989), or $P_{\text{mag}} \approx 7200 \text{ cm}^{-3} \text{ pc}$. This is larger than the thermal pressure in the WIM (KH), but only by a factor of 1.8. The line width of the WIM is unlikely to be super-Alfvénic, because a large energy input would be required to maintain the large line width. Thus, the WIM is probably not dominated by magnetic pressure to a very large extent, in contrast to the well-defined H I shells.

e) Filaments versus Shells

This paper's fairly close look at a few H I shells has led us to conclude that the morphologically distinct H I structures we see are filaments, not edge-on shells. The dominance of magnetic pressure in the filaments perhaps suggests that the formation of a filament in an expanding H I shell is related to the existence of the magnetic field, and from the purely geometrical standpoint it is natural to assume that the filament axis lies along the only preferred direction in the region, namely, along

the magnetic field direction. However, this is contrary to theoretical expectation: when magnetic pressure dominates gas pressure, gas condensation perpendicular to the field lines is inhibited. Unfortunately, we cannot observationally resolve this question, because we cannot determine the relative orientation of the magnetic field with respect to the filament axis.

IX. SUMMARY

We have measured B_{\parallel} from the Zeeman effect for the 21 cm line in emission in a number of morphologically prominent H I shells. The H I structures are, in fact, filamentary instead of sheetlike. B_{\parallel} is typically $\sim 6.4 \mu\text{G}$. If our estimates of n_{HI} are correct, magnetic pressure dominates thermal gas pressure by a factor ~ 67 , and line widths are somewhat smaller than the Alfvén velocity. Troland and Heiles (1982*b*) interpreted the results for one position in the Eridanus shell in terms of an isothermal shock, and this interpretation should apply reasonably well for all of the shells examined here.

The Zeeman effect is much more difficult to detect in Simard-Normandin and Kronberg's (1980) region A, which serves a control region in which H I shell structure is not morphologically prominent. The average $\langle |B_{\parallel}| \rangle$ is smaller in this region (Fig. 7) than in well-defined H I shells by a factor of about 1.9 or more, the uncertainty arising from the definition of "well defined." We conclude that the field is amplified in shell structures.

B_{\parallel} , as derived from the Zeeman effect, does not correlate with Faraday rotation. A similar lack of correlation is found when comparing optical and diffuse synchrotron polarization in the North Polar Spur. Thus, the magnetic field is oriented differently in different types of region, with little if any correlation. The magnetic field plays a leading dynamical role in the H I and probably minor one in the WIM, where Faraday rotation is produced.

In the process of deriving B_{\parallel} we decomposed the I spectrum for every position into Gaussian components. Most positions require a broad Gaussian, which presumably corresponds to the "warm neutral medium" (WNM). FWHMs for many of these components require temperatures less than a few thousand K. Gas at such temperatures is thermally unstable. This situation desperately needs further investigation along the lines suggested in § VIIIc.

This work was supported in part by a National Science Foundation grant to the author. Operation of the HCRO is also supported by the NSF.

REFERENCES

- Arons, J., and Max, C. E. 1975, *Ap. J. (Letters)*, **196**, L77.
 Berkhuysen, E. M. 1973, *Astr. Ap.*, **24**, 143.
 Berkhuysen, E. M., Haslam, C. G. T., and Salter, C. M. 1971, *Astr. Ap.*, **14**, 252.
 Colomb, F. R., Pöppel, W. G. L., and Heiles, C. 1980, *Astr. Ap. Suppl.*, **40**, 47.
 Cox, D. P. 1987, in *IAU Colloquium 101, Supernova Remnants and the Interstellar Medium*, ed. R. S. Roger and T. L. Landecker (Cambridge: Cambridge University Press), p. 73.
 Elmegreen, B. G. 1985, *Ap. J.*, **299**, 196.
 Falgarone, E., and Puget, J. L. 1986, *Astr. Ap.*, **162**, 235.
 Field, G. B. 1965, *Ap. J.*, **142**, 531.
 Heiles, C. 1975, *Astr. Ap. Suppl.*, **20**, 37.
 ———. 1976, *Ap. J. (Letters)*, **208**, L137.
 ———. 1979, *Ap. J.*, **239**, 533.
 ———. 1984*a*, *Ap. J. Suppl.*, **55**, 585.
 ———. 1984*b*, in *IAU Colloquium Local Interstellar Medium*, ed. Y. Kondo, F. C. Bruhweiler, and B. D. Savage (NASA Conf. Pub. 2345), p. 263.
 ———. 1987, in *Interstellar Processes*, ed. D. J. Hollenbach and H. A. Thronson, Jr. (Dordrecht: Reidel), p. 171.
 ———. 1988, *Ap. J.*, **324**, 321.
 Heiles, C., Chu, Y.-H., Reynolds, R. J., Yegingil, I., and Troland, T. H. 1980, *Ap. J.*, **242**, 533.
 Heiles, C., and Habing, H. J. 1974, *Astr. Ap. Suppl.*, **14**, 1.
 Heiles, C., and Troland, T. H. 1982, *Ap. J. (Letters)*, **260**, L23.
 Kraus, J. D. 1966, *Radio Astronomy* (New York: McGraw-Hill).
 Kulkarni, S., and Heiles, C. 1987, in *Interstellar Processes*, ed. D. J. Hollenbach and H. A. Thronson, Jr. (Dordrecht: Reidel), p. 87.
 ———. 1988, in *Galactic and Extragalactic Radio Astronomy*, ed. G. L. Verschuur and K. Kellermann (Berlin: Springer), p. 95.
 Mebold, U. 1972, *Astr. Ap.*, **19**, 13.
 Myers, P. C., and Goodman, A. A. 1988, *Ap. J. (Letters)*, **326**, L27.
 Rand, R. J., and Kulkarni, S. R. 1989, *Ap. J.*, submitted.
 Reynolds, R. J., and Ogden, P. M. 1979, *Ap. J.*, **229**, 942.
 Shu, F. H., Adams, F. C., and Lizano, S. 1987, *Ann. Rev. Astr. Ap.*, **25**, 23.
 Simard-Normandin, M., and Kronberg, P. P. 1980, *Ap. J.*, **242**, 74.
 Simard-Normandin, M., Kronberg, P. P., and Butten, S. 1981, *Ap. J. Suppl.*, **45**, 97.
 Spoelstra, T. A. Th. 1971, *Astr. Ap.*, **13**, 237.
 ———. 1972, *Astr. Ap.*, **21**, 61.

Troland, T. H., and Heiles, C. 1982a, *Ap. J.*, **252**, 179.
———, 1982b, *Ap. J. (Letters)*, **260**, L19.
Verschuur, G. L. 1969, *Ap. J.*, **156**, 861.

Verschuur, G. L., and Schmelz, J. T. 1988, *A.J.*, submitted.
Zweibel, E. G., and Josafatsson, K. 1983, *Ap. J.*, **270**, 511.

CARL HEILES: Astronomy Department, University of California Berkeley, CA 94720